NASA TECHNICAL MEMORANDUM TM 88523

DIRECT CALCULATION OF WALL INTERFERENCES AND WALL ADAPTATION FOR TWO-DIMENSIONAL FLOW IN WIND TUNNELS WITH CLOSED WALLS

Juergen Amecke

Translation of "Direkte Berechnung von Wandinterferenzen und Wandadaption bei zweidimensionaler Stroemung in Windkanaelen mit geschlossenen Waenden," DFVLR Institut fuer Experimentelle Stroemungsmechanik, Goettingen, West Germany, Nov. 1985

NATIONAL AERONAUTICS AND SPACE ADMINISTRATION

WASHINGTON, D.C. 20546 DEC. 1986

STANDARD TITLE PAGE

1. Report No.	2. Government Accession No.	3. Recipient's Catalog No.
TM 88523		

4. Title and Subtitle	5. Report Date
Direct Calculation of Wall Interferences and wall adaptation for two-dimensional flow in wind tunnels with closed walls	Dec. 86
	6. Performing Organization Code
7. Author(s)	8. Performing Organization Report No.
J. Amecke	10. Work Unit No.
9. Performing Organization Name and Address	11. Contract or Grant No.
	13. Type of Report and Period Covered
12. Sponsoring Agency Name and Address	14. Sponsoring Agency Code

15. Supplementary Notes

Translation of "Direkte Berechnung von Wandinterferenzen und Wandadaption bei zweidimensionaler Stroemung in Windkanaelen mit geschlossenen Waenden," DFVLR Institut fuer Experimentelle Stroemungsmechanik, Goettingen, West Germany, Nov. 1985

16. Abstract

Based on Cauchy's integral formula, a method has been derived for direct calculation of the wall-induced interference velocity in two-dimensional flow. This 'one step' method allows the calculation of the residual corrections and the required wall adaptation for interference-free flow from the wall pressure distribution without any model representation. Several applications are demonstrated by examples.

17. Key Words [Selected by Author(s)]	18. Distribution Statement
	Unclassified-Unlimited

19. Security Classif.(of this report)	20. Security Classif. (of this page)	21. No. of pages	22.
Unclassified	Unclassified	93	

Summary

Based on Cauchy's integral formula, a method has been derived for direct calculation of the wall-induced interference velocity in two-dimensional flow. This 'one step' method allows the calculation of the residual corrections and the required wall adaptation for interference-free flow from the wall pressure distribution without any model representation. Several applications are demonstrated by examples.

Contents

Abbreviations

B	Width of measurement lane
c_A	Coefficient of lift
c_W	Coefficient of friction
H	Height of measurement lane
L	Depth of profile
Ma	Mach number
R	Radius of circular cylinder as model
r	Distance from coordinate origin
U	Velocity component in x-direction
u	Dimensionless interference velocity in x-direction (equation 8)
V	Velocity component in y-direction
v	Dimensionless interference velocity in y-direction (equation 8)
x,y	Coordinates of the lift point in the measurement lane
z	Complex coordinate of the lift point (eq. 3)
α	Angle of attack
$\beta = \sqrt{1-Ma_\infty^2}$	Prandtl factor
ΔH	Deflection of Measurement lane wall for adaptation
ΔMa	Mach number correction due to wall influence
$\Delta\alpha$	Correction to angle of attack due to wall influence
ζ	Complex coordinate of the running point (equation 2)
ξ,η	Coordinates of the running point on the boundary C

Superscripts

i	Induced by measurement lane wall (wall interference)
m	Induced by the model

Subscripts

a	Measurement lane outlet
c	On the boundary c
e	Measurement lane inlet
m	Measurement lane axis
o	Upper wall of measurement lane
u	Lower wall of measurement lane
∞	Basic flow

1. Introduction

A moving airplane wing profile generates turbulance in the surrounding flow medium, which decays slowly outward with increasing distance from the model. If such a model is to be investigated in a wind tunnel, then the described flow field is affected by the boundary dimensions of the stream or by the wind tunnel walls. These wall influences or wall interferences are not desirable if the problem is to investigate the flow around a model in infinite space.

The measured result is then independent of the specific properties of the test facility only if one can describe the wall interference.

Thus one must attempt either to suppress the wall interferences through an actual wall structure, or to correct the measured results so that they are free of wall influences.

When limited to a two-dimensional, friction-free flow, a method for calculating the wall interferences can be derived from the Cauchy integral formula solely from the wall pressure distribution and the wall contour. Data on the form or position of the model in the measurement lane (model conception) are not a part of the calculation.

The algorithm makes possible a direct determination of wall-induced interference velocity in every point of the flow field.

The result can be used either to deform the walls so that the model has interference-free flow (wall adaptation), or it can be

used to correct the measured results so that they are affected as little as possible by wall interference (residual correction).

The present paper deals with the wall interferences in wind tunnels with closed walls of any shape using two-dimensional flow. Wall interferences in wind tunnels with partly open walls (preferrably slit) are reserved for a future paper.

2. Calculation of Wall Induced Interference Velocity

2.1 Infinite Measurement Lane

A direct calculation of wall induced interference velocity is possible by using the Cauchy integral formula*:

$$f(z) = \frac{1}{2\pi i} \oint_C \frac{f(\zeta)}{\zeta - z} \, d\zeta . \tag{1}$$

Here, C is the closed wall around any region. When applied to the flow in the measurement lane of a wind tunnel, C should enclose the model and run near or in the wall. The region enclosed upstream and downstream is arbitrary (Fig. 1). For simplification of the subsequent derivation however, it is initially assumed that C upstream and downstream lie in the undisturbed inflow or outflow. By using the complex flow function, we obtain the following expression for the running point on the wall edge C:

---

*Reference to the Cauchy integral formula and its favorable properties specifically for this application was supplied by Dr. E. Wedemeyer. In the meantime, several papers have been published which treat the problem similarly. A summary of all recent papers in the area of two-dimensional wind tunnel wall interference is found in [1].

(2) $$\zeta = \xi + i\,\eta; \qquad f(\zeta) = u_c - i\,v_c$$

and for any, random point within the boundary C:

(3) $$z = x + i\,y; \qquad f(z) = u - i\,v.$$

From the definition of the argument via the complex flow function, it follows that all solutions of the Cauchy integral formula are also solutions of the potential equation.

By using the Cauchy residue equation, one can show in general [2,3,4] that singularities in the interior of the boundary region C add no amount to the integral.

If one assumes that the flow field in a closed measurement lane can be described as an overlap of the velocity field induced by the model in infinite space, and of the interference flow field induced as a rection with the walls, then we conclude that the model can be described by singularities within C alone, and the wall interferences can be described by singularities outside C alone. Since in the Cauchy integral formula only the singularities outside C provide any contribution, it directly gives the wall induced interference velocity at every point within C. In the given form, the Cauchy integral formula applies only for incompressible flows. By distortion of the flow field per the Gothert rule [5], the method can also be expanded for the compressible subsonic range. With the Prandtl factor

(4) $$\beta = \sqrt{1-Ma_\infty^2}$$

we obtain:

(5) $$\zeta = \xi + i\,\beta\,\eta; \qquad f(\zeta) = \beta^2\,u_c - i\,\beta\,v_c$$

(6) $$z = x + i\,\beta\,y; \qquad f(z) = \beta^2 u - i\,\beta\,v.$$

The Gothert rule applies only for the linearized potential equation. But this means in general, no limitation in the calculation of wall induced interference velocity, since even in a highly non-linear flow field in the region of the model (local supersonic fields, cavitation), one can assume that the turbulance near the wall (on the boundary C, the integration path) has decreased so much that a linearized treatment is permitted (Fig. 1).

The following definitions apply for the dimensionless turbulance velocities in the linearized potential equation:

(7) $$u_c = \frac{U_c}{U_\infty} - 1; \qquad v_c = \frac{V_c}{U_\infty}$$

(8) $$u = \frac{U}{U_\infty} - 1; \qquad v = \frac{V}{U_\infty}.$$

By introduction of eq. (5) and (6) into the Cauchy integral formula eq. (1), after rearrangement of the numerator we obtain the following relation for the wall-induced interference velocity:

(9) $$\beta u^i - i\,v^i = \frac{1}{2\pi i}\oint_C \frac{\beta\,u_c - i\,v_c}{(\zeta - x) + i\,\beta\,(\eta - y)}\, d(\xi + i\,\beta\,\eta).$$

After expansion:

(10) $$u^i - i\,\frac{v^i}{\beta} = -\frac{1}{2\pi}\oint_C \frac{[\,i(\xi - x) + \beta\,(\eta - y)\,]\,(u_c - i\,\frac{v_c}{\beta})}{(\xi - x)^2 + \beta^2(\eta - y)^2}\, d(\xi + i\beta\eta)$$

and multiplying out, the integral can be split into real and imaginary parts:

$$u^i = -\frac{\beta}{2\pi}\oint_C \frac{u_c\,(\eta - y) + \frac{v_c}{\beta^2}\,(\xi - x)}{(\xi - x)^2 + \beta^2\,(\eta - y)^2}\, d\xi +$$

(11a)

$$+\frac{\beta}{2\pi}\oint_C \frac{u_c\,(\xi - x) - v_c\,(\eta - y)}{(\xi - x)^2 + \beta^2\,(\eta - y)^2}\, d\eta$$

$$v^i = \frac{\beta}{2\pi} \oint_C \frac{u_c\,(\xi-x) - v_c\,(\eta-y)}{(\xi-x)^2 + \beta^2\,(\eta-y)^2}\,d\xi +$$

(11b)

$$+ \frac{\beta}{2\pi} \oint_C \frac{u_c\,\beta^2(\eta-y) + v_c(\xi-x)}{(\xi-x)^2 + \beta^2\,(\eta-y)^2}\,d\eta\,.$$

Of the many different potential applications of this equation, we will first discuss the case of an infinite measurement lane with closed, slightly curved walls. The integration region shall extend from the undisturbed inflow to the undisturbed outflow. Since in this case the inflow and outflow cross-section provide no contribution to the integral, only two line integrals are left. With

$$\eta = \pm\, H/2 \quad \text{(boundary C on the wall)}$$

from eq. (11) we obtain:

(12a)

$$u^i = + \frac{\beta}{2\pi} \int_{-\infty}^{\infty} \frac{u_u\,(\frac{H}{2}+y) - \frac{v_u}{\beta^2}\,(\xi-x)}{(\xi-x)^2 + \beta^2\,(\frac{H}{2}+y)^2}\,d\xi +$$

$$+ \frac{\beta}{2\pi} \int_{-\infty}^{\infty} \frac{u_o\,(\frac{H}{2}-y) + \frac{v_o}{\beta^2}\,(\xi-x)}{(\xi-x)^2 + \beta^2\,(\frac{H}{2}-y)^2}\,d\xi$$

$$v^i = \frac{\beta}{2\pi} \int_{-\infty}^{\infty} \frac{u_u\,(\xi-x) + v_u\,(\frac{H}{2}+y)}{(\xi-x)^2 + \beta^2\,(\frac{H}{2}+y)^2}\,d\xi -$$

(12b)

$$- \frac{\beta}{2\pi} \int_{-\infty}^{\infty} \frac{u_o\,(\xi-x) - v_o\,(\frac{H}{2}-y)}{(\xi-x)^2 + \beta^2\,(\frac{H}{2}-y)^2}\,d\xi\,.$$

Depending on the assumptions, u^i and v^i are the components of wall induced interference velocity at any point (x, y) within a measurement lane. The most important special case obtained above is the wall induced interference velocity on the measurement lane axis (y = 0):

(13a)
$$u_m^i = \frac{\beta}{2\pi} \int_{-\infty}^{\infty} \frac{(u_u+u_o)\,\frac{H}{2} + \frac{v_o-v_u}{\beta^2}\,(\xi-x)}{(\xi-x)^2 + \beta^2\,(\frac{H}{2})^2}\,d\xi$$

(13b)
$$v_m^i = \frac{\beta}{2\pi} \int_{-\infty}^{\infty} \frac{(u_u-u_o)\,(\xi-x) + (v_o+v_u)\,\frac{H}{2}}{(\xi-x)^2 + \beta^2\,(\frac{H}{2})^2}\,d\xi\,.$$

The integration extends over two straight, parallel lines on which a finite v-component (i.e. wall slope) is allowed. This procedure is justified, as long as the wall deflection is small compared with the tunnel height, i.e.

$$H >> \Delta H.$$

For a straight (not adapted) wall, the v-components in eq. (13) disappear.

2.2 Finite Measurement Lane

In the calculation presented in Section 2.1 it was assumed that the integration path extends infinitely upstream and downstream. This is only justified in measurment lanes which are so long that the interference velocities diminish entirely. Application of the Cauchy integral formula to a finite measurement lane

requires a closed line segment (see Fig. 1) which intersects the flow field upsteam and downstream from the model.

To do so, eq. (11) is divided below into line integrals:

$$
\begin{aligned}
u^i = &+\frac{\beta}{2\pi}\int_{x_e}^{x_a}\frac{u_u\left(\frac{H}{2}+y\right)-\frac{v_u}{\beta^2}(\xi-x)}{(\xi-x)^2+\beta^2\left(\frac{H}{2}+y\right)^2}\,d\xi+\\
&+\frac{\beta}{2\pi}\int_{x_e}^{x_a}\frac{u_o\left(\frac{H}{2}-y\right)+\frac{v_o}{\beta^2}(\xi-x)}{(\xi-x)^2+\beta^2\left(\frac{H}{2}-y\right)^2}\,d\xi-\\
&-\frac{\beta}{2\pi}\int_{-\frac{H}{2}}^{\frac{H}{2}}\frac{u_e(x_e-x)-v_e(\eta-y)}{(x_e-x)^2+\beta^2(\eta-y)^2}\,d\eta+\\
&+\frac{\beta}{2\pi}\int_{-\frac{H}{2}}^{\frac{H}{2}}\frac{u_a(x_a-x)-v_a(\eta-y)}{(x_a-x)^2+\beta^2(\eta-y)^2}\,d\eta
\end{aligned}
\tag{14a}
$$

$$
\begin{aligned}
v^i = &\frac{\beta}{2\pi}\int_{x_e}^{x_a}\frac{u_u(\xi-x)+v_u\left(\frac{H}{2}+y\right)}{(\xi-x)^2+\beta^2\left(\frac{H}{2}+y\right)^2}\,d\xi-\\
&-\frac{\beta}{2\pi}\int_{x_e}^{x_a}\frac{u_o(\xi-x)-v_o\left(\frac{H}{2}-y\right)}{(\xi-x)^2+\beta^2\left(\frac{H}{2}-y\right)^2}\,d\xi-\\
&-\frac{\beta}{2\pi}\int_{-\frac{H}{2}}^{\frac{H}{2}}\frac{u_e\beta^2(\eta-y)+v_e(x_e-x)}{(x_e-x)^2+\beta^2(\eta-y)^2}\,d\eta+\\
&+\frac{\beta}{2\pi}\int_{-\frac{H}{2}}^{\frac{H}{2}}\frac{u_a\beta^2(\eta-y)+v_a(x_a-x)}{(x_a-x)^2+\beta^2(\eta-y)^2}\,d\eta\,.
\end{aligned}
\tag{14b}
$$

Eq. (14) requires a knowledge of the velocity profile in the inflow and outflow. If instead, a constant interference velocity

can be assumed in the inflow and outflow, then the corresponding integrals have closed solutions [8]. Since the integrals are of similar structure, it is enough to use the u-component in the outlet as an example (designations see Fig. 1):

$$u_a = \text{const.} \qquad v_a = \text{const.}$$

(15)
$$\frac{\beta}{2\pi} \int_{-\frac{H}{2}}^{\frac{H}{2}} \frac{u_a\,(x_a-x) + v_a\,(\eta-y)}{(x_a-x)^2 + \beta^2\,(\eta-y)^2}\,d\eta =$$

$$= \frac{u_a}{2\pi}\ \text{arctg}\ \frac{\beta\,H\,(x_a-x)}{(x_a-x)^2 - \beta^2\,[(\frac{H}{2})^2 - y^2]} + \frac{v_a}{4\pi\beta}\ \ln \frac{(x_a-x)^2 + \beta^2\,(\frac{H}{2}-y)^2}{(x_a-x)^2 + \beta^2\,(\frac{H}{2}+y)^2}\ .$$

If we introduce this simplification into eq. (14), we obtain the following expression for the special case of wall induced interference velocity on the tunnel axis (y = 0) corresponding to eq. (13):

(16a)
$$u_m^i = \frac{\beta}{2\pi} \int_{x_e}^{x_a} \frac{(u_o+u_u)\,\frac{H}{2} + \frac{v_o-v_u}{\beta^2}\,(\xi-x)}{(\xi-x)^2 + \beta^2\,(\frac{H}{2})^2}\,d\xi -$$

$$- \frac{u_e}{2\pi}\ \text{arctg}\ \frac{\beta\,H\,(x_e-x)}{(x_e-x)^2 - \beta^2\,(\frac{H}{2})^2} + \frac{u_a}{2\pi}\ \text{arctg}\ \frac{\beta\,H\,(x_a-x)}{(x_a-x)^2 - \beta^2\,(\frac{H}{2})^2}$$

(16b)
$$v_m^i = \frac{\beta}{2\pi} \int_{x_e}^{x_a} \frac{(u_u-u_o)\,(\xi-x) + (v_o+v_u)\,\frac{H}{2}}{(\xi-x)^2 + \beta^2\,(\frac{H}{2})^2}\,d\xi -$$

$$- \frac{v_e}{2\pi}\ \text{arctg}\ \frac{\beta\,H\,(x_e-x)}{(x_e-x)^2 - \beta^2\,(\frac{H}{2})^2} + \frac{v_a}{2\pi}\ \text{arctg}\ \frac{\beta\,H\,(x_a-x)}{(x_a-x)^2 - \beta^2\,(\frac{H}{2})^2}\ .$$

3. Calculation of Wall Induced Interference Velocity at the Wall

3.1 Infinite Measurement Lane

By using the Cauchy integral formula, the wall induced interference velocity can be calculated both within the boundary C (Fig. 1) and also on the boundary itself. The latter can be used for adaptive wind tunnel walls, since the computed v-component of the interference velocity can be compensated by an equivalent, opposing change in wall slope.

Since within the agreed assumptions, we are dealing with a precise method, the adaptation takes place in one step.

Proceeding from eq. (12) we obtain the following expression when approaching the lift point at the upper wall:

i.e. y --> H/2 or = H/2 - y --> 0:

(17a)

$$u_o^i = + \frac{\beta}{2\pi} \int_{-\infty}^{\infty} \frac{u_u H - \frac{v_u}{\beta^2}(\xi - x)}{(\xi - x)^2 + \beta^2 H^2} d\xi + \frac{\beta}{2\pi} \int_{-\infty}^{\infty} \frac{u_o \epsilon + \frac{v_o}{\beta^2}(\xi - x)}{(\xi - x)^2 + \beta^2 \epsilon^2} d\xi$$

$$v_o^i = \frac{\beta}{2\pi} \int_{-\infty}^{\infty} \frac{u_u(\xi - x) + v_u H}{(\xi - x)^2 + \beta^2 H^2} d\xi -$$

(17b)

$$- \frac{\beta}{2\pi} \int_{-\infty}^{\infty} \frac{u_o(\xi - x) - v_o \epsilon}{(\xi - x)^2 + \beta^2 \epsilon^2} d\xi .$$

Since ε tends to zero, the corresponding integrands are singular at $\xi \dashrightarrow x$. The value of the integral must then be specified by another boundary crossing (Cauchy primary value). The following partial integrals from eq. (17a) must be investigated:

a) Partial integral I_1

$$I_1 = \frac{\beta}{2\pi} \int_{-\infty}^{\infty} \frac{u_o \, \varepsilon}{(\xi - x)^2 + (\beta\varepsilon)^2} \, d\xi \tag{18}$$

It is initially assumed that u_o is constant within the integration bounds. We then obtain:

$$I_1 = \frac{u_o}{2\pi} \int_{-\infty}^{\infty} \frac{\beta \, \varepsilon}{(\xi - x)^2 + (\beta\varepsilon)^2} \, d\xi \tag{19}$$

$$= \frac{u_o}{2\pi} \left[\text{arc tg} \, \frac{\xi - x}{\beta \, \varepsilon} \right]_{-\infty}^{\infty} \tag{20}$$

Regardless of $\beta\varepsilon$, for the given integration limits we obtain:

$$I_1 = \frac{u_o}{2} . \tag{21}$$

The integrand of eq. (19) is illustrated in Fig. 2 for various values of $\beta\varepsilon$. We see that the integrand is different only at the singular point of zero, with decreasing $\beta\varepsilon$. The assumption u_o = const. thus is not a limitation for the result.

b) Partial integral I_2

(22) $$I_2 = \frac{\beta}{2\pi} \int_{-\infty}^{\infty} \frac{\frac{v_o}{\beta^2}(\xi - x)}{(\xi - x)^2 + (\beta\epsilon)^2} \, d\xi \, .$$

The integrand of eq. (22) is illustrated in Fig. 3 for v_o = const. The functional value at the singular point is always zero, regardless of $\beta\epsilon$.

A numerical integration causes no difficulties, if the integration interval is chosen small enough, and one strip on each side of the singular point is separated out.

In the boundary case: $\beta\epsilon \dashrightarrow 0$, we then have:

(23) $$I_2 = \frac{1}{2\pi\beta} \left(\int_{-\infty}^{\xi - x = 0} \frac{v_o}{\xi - x} \, d\xi + \int_{\xi - x = 0}^{\infty} \frac{v_o}{\xi - x} \, d\xi \right) .$$

By application of eq. (21) and eq. (23), we obtain from eq. (17):

(24a) $$u_o^i = \frac{\beta}{2\pi} \int_{-\infty}^{\infty} \frac{u_u H - \frac{v_u}{\beta^2}(\xi - x)}{(\xi - x)^2 + \beta^2 H^2} \, d\xi + \frac{u_o}{2} + \frac{1}{2\pi\beta} \int_{-\infty + (\xi - x = 0)}^{\xi - x = 0)} \frac{v_o}{\xi - x} \, d\xi$$

(24b) $$v_o^i = \frac{\beta}{2\pi} \int_{-\infty}^{\infty} \frac{u_u (\xi - x) + v_u H}{(\xi - x)^2 + \beta^2 H^2} \, d\xi + \frac{v_o}{2} - \frac{\beta}{2\pi} \int_{-\infty + (\xi - x = 0)}^{\xi - x = 0)} \frac{u_o}{\xi - x} \, d\xi \, .$$

Similarly, we obtian expressions for the lower wall:

$$u_u^i = \frac{\beta}{2\pi}\int_{-\infty}^{\infty} \frac{u_o H + \frac{v_o}{\beta^2}(\xi - x)}{(\xi - x)^2 + \beta^2 H^2}\, d\xi + \left| \begin{array}{l} (\xi - x = 0) + \infty \\ + \frac{u_u}{2} - \frac{1}{2\pi\beta}\int \frac{v_u}{(\xi - x)}\, d\xi \\ -\infty + (\xi - x = 0) \end{array} \right. \tag{25a}$$

$$v_u^i = \frac{\beta}{2\pi}\int_{-\infty}^{\infty} \frac{u_o(\xi - x) - v_o H}{(\xi - x)^2 + \beta^2 H^2}\, d\xi + \left| \begin{array}{l} (\xi - x = 0) + \infty \\ + \frac{v_u}{2} + \frac{\beta}{2\pi}\int \frac{u_u}{\xi - x}\, d\xi \, . \\ -\infty + (\xi - x = 0) \end{array} \right. \tag{25b}$$

The v-components of the wall-induced interference velocity, eq. (23b) and eq. (24b), are the needed wall slope change if the wall is to be adapted. Since only small wall slopes are handled in a linearized treatment of the flow field, we have:

$$d(\Delta H)/dx = v, \text{ when } u << 1.$$

Accordingly, we obtain the profile of the wall flow line through integration:

$$\Delta H = \int_{x_e}^{x} v\, dx \, . \tag{26}$$

The starting point of the integration can be set arbitrarily.

3.2 Finite Measurement Lane

From the relations derived above, formulas can now be determined for the missing case, namely of wall induced interference velocity on a wall for a finite length measurement lane.

If the velocity profile in the inlet and outlet flow is known, then the interference velocity is computed from eq. (14) with the Cauchy primary values corresponding to eq. (21) and eq. (23). Therefore, an explicite presentation of formulas can be omitted at this point. Regarding eq. (21) note that it also follows from the integral solution eq. (20), when the integration limits are finite, but $\beta \varepsilon$ tend toward zero.

If we can postulate a constant velocity in the inlet or outlet flow, then from eq. (25) and eq. (15) we obtain the following relation (y = H/2):

$$u_o^i = \frac{\beta}{2\pi} \int_{x_e}^{x_a} \frac{u_u H - \frac{v_u}{\beta^2}(\xi - x)}{(\xi - x)^2 + \beta^2 H^2} d\xi + \frac{u_o}{2} + \frac{1}{2\pi\beta} \int_{x_e + (\xi - x = 0)}^{(\xi - x = 0) + x_a} \frac{v_o}{\xi - x} d\xi - \tag{27a}$$

$$- \frac{u_e}{2\pi} \operatorname{arc\,tg} \frac{\beta H}{x_e - x} + \frac{u_a}{2\pi} \operatorname{arc\,tg} \frac{\beta H}{x_a - x} +$$

$$+ \frac{v_e}{4\pi\beta} \ln \frac{(x_e - x)^2}{(x_e - x)^2 + \beta^2 H^2} - \frac{v_a}{4\pi\beta} \ln \frac{(x_a - x)^2}{(x_a - x)^2 + \beta^2 H^2}$$

$$v_o^i = -\frac{\beta}{2\pi}\int_{x_e}^{x_a} \frac{u_u\,(\xi-x) + v_u\,H}{(\xi-x)^2 + \beta^2 H^2}\,d\xi + \frac{v_o}{2} + \frac{\beta}{2\pi}\int_{x_e}^{(\xi - x = 0) \to x_a} \frac{u_o}{\xi-x}\,d\xi -$$

(27b)
$$- \frac{v_e}{2\pi}\,\text{arc tg}\,\frac{\beta\,H}{x_e-x} + \frac{v_a}{2\pi}\,\text{arc tg}\,\frac{\beta\,H}{x_a-x} -$$

$$- \frac{u_e\beta}{4\pi}\,\ln\,\frac{(x_e-x)^2}{(x_e-x)^2 + \beta^2 H^2} + \frac{u_a\beta}{4\pi}\,\ln\,\frac{(x_a-x)^2}{(x_a-x)^2 + \beta^2 H^2}.$$

Similarly, we obtain the interference velocity on the lower wall.

4. Wall Adaptation for Simple Singularity Arrangements

4.1 Circular Cylinder (Dipole)

Application of the Cauchy integral formula to the calculation of wall adaptations will be illustrated first on several simple examples for incompressible flow. We begin with the overlap of translational flow and dipole in a tunnel. Evidently this corresponds to a non-friction flow around a circular cylinder.

By overlapping the flow fields of the dipole in the measurement lane (Fig. 4) and by overlapping an infinite series of reflected dipoles, the straight tunnel wall becomes a flow line.

A single dipole in the coordinate origin induces turbulence velocity components at any random point of the flow field [6]:

(28a)
$$u = \frac{R^2}{r^2}\,\frac{y^2-x^2}{r^2}$$

(28b)
$$v = -2\,\frac{R^2}{r^2}\,\frac{x\,y}{r^2}.$$

The stagnation point flow line of the dipole in a parallel flow is a circle of radius R. For a point on the upper wall (y = H/2) we then obtain:

(29a) $$u = 4 \left(\frac{R}{H}\right)^2 \frac{1 - \left(2\frac{x}{H}\right)^2}{\left[1+\left(2\frac{x}{H}\right)^2\right]^2}$$

(29b) $$v = -8 \left(\frac{R}{H}\right)^2 \frac{2\frac{x}{H}}{\left[1+\left(2\frac{x}{H}\right)^2\right]^2} .$$

For all dipoles we obtain the following (converging) series from eq. (29a):

(30) $$u = 8 \left(\frac{R}{H}\right)^2 \left(\frac{1^2-\left(2\frac{x}{H}\right)^2}{\left[1^2+\left(2\frac{x}{H}\right)^2\right]^2} + \frac{3^2-\left(2\frac{x}{H}\right)^2}{\left[3^2+\left(2\frac{x}{H}\right)^2\right]^2} + \frac{5^2-\left(2\frac{x}{H}\right)^2}{5^2+\left(2\frac{x}{H}\right)^2\right]^2} + \ldots\right).$$

In [7] we find the sum expression for this series:

(31) $$u = \left(\frac{\pi}{\frac{H}{R}\cosh\left(\pi\frac{x}{H}\right)}\right)^2.$$

From eq. (31) the wall velocity $u_{o,u}$ is computed for R/H = 0.133 as an example, and this is entered as a dashed line in Fig. 5 (bottom). The velocity component in the y-direction $v_{o,u}$ and the wall deflection ΔH are postulated as zero.

When applying the computation method derived in Section 2 to determine the wall induced interference velocities, these dashed curves can be viewed as "measured results" for which a wall adaptation is to be performed.

By eq. (13) the wall induced interference velocities on the measurement lane axis $u_m^i;\ v_m^i$

are computed and entered in Fig. 5 (top).

By eq. (24) the wall induced interference velocities are determined at the location of the upper and lower wall:

$$u^i_{o,u};\ v^i_{o,u}$$

The given flow field is the overlap of the flow field induced by the model, and of the interference flow field induced by the walls. Accordingly, for the interference-free flow, we have:

(32a) $$u^m_{o,u} = u_{o,u} - u^i_{o,u}$$

(32b) $$v^m_{o,u} = \quad - v^i_{o,u}$$

Moreover, by integration of the v-components per eq. (26), we obtain the profile of the flow line ΔH, the "adapted" wall contour. In Fig. 5 (middle) the components of the interference-free flow and the adapted wall contour are shown by solid lines. Compared with the given, straight wall, the adapted contour forms a symmetrical expansion of the measurement lane in the region of the model and connected with this, the wall velocity $u_{o,u}$ decreases.

As a check, the interference flow around a single dipole can be computed directly from eq. (28) and it then agrees with the illustrated results.

4.2 Potential Eddy

While the above investigated dipole flow can be viewed as an example for a friction-free flow around compressible bodies, the

overlapping of potential eddys and translation is an example for a body with lift without compression.

We proceed as before. A single, potential eddy at the coordinate origin induces the following interference velocity components at any point of the flow field [6]:

(33a) $$u = \frac{c_A L}{4\pi} \frac{y}{x^2+y^2}$$

(33b) $$v = \frac{c_A L}{4\pi} \frac{x}{x^2+y^2} .$$

By overlapping the potential eddy in the measurement lane (Fig. 6) and overlapping an infinite series of reflected eddys outside the measurement lane, the tunnel wall becomes a flow line.

From eq. (33a) we obtain the following (converging) series for a point on the upper wall (y = H/2):

(34) $$u = \frac{c_A}{\pi \frac{H}{L}} \left[\frac{1}{1+(2\frac{x}{H})^2} - \frac{3}{3^2+(2\frac{x}{H})^2} + \frac{5}{5^2+(2\frac{x}{H})^2} \pm \ldots \right].$$

In [7] we find the sum expression for this series:

(35) $$u = \frac{c_A}{4 \frac{H}{L} \cosh(\pi \frac{x}{H})} .$$

In Fig. 7 (bottom) the wall velocity distribution determined with eq. (35) for $c_A = 0.8$ is plotted as an example. At the upper wall, we obtain an excess velocity (turbulent velocity positive) and at the lower wall a decreased velocity (turbulent velocity

negative). As assumed, the normal components of the turbulent velocity and the wall deflection are zero.

By using eq. (13) the wall induced interference velocity was determined on the measurement lane axis and plotted in Fig. 7 (top).

By using eq. (24), the wall induced interference velocity can be computed at the location of the wall. With eq. (26) we obtain from the normal component, the profile of the "adapted" wall contour. The beginning of integration is (arbitrarily) set at $x_e/L = -4$.

Due to the missing compression effect of the potential eddy, the two measurement lane walls are deformed in parallel.

Other illustrative examples are obtained by overlapping dipole and potential eddy corresponding to the flow about a circular cylinder with circulation. Two examples with the same circulation ($c_A = 0.8$) but differing compression effect are illustrated in Figures 8 and 9.

In these examples, the typical properties of a profile flow are containd (compression and lift). Thus later, in the treatment of real profile flows, we fill find similar curve segments.

5. Incompletely Adapted Walls

5.1 Error Estimation

In Figures 7 to 9 we see that for a complete compensation of the interference velocity, the measurement lane walls must be

adapted over a considerable length. In particular we see that a much longer measurement lane is needed for bodies with lift, than for pure compression bodies without lift. This observation is confirmed by the different decay behavior of the indcued normal component x >> y:

Dipole (eq. 28b): $v \sim 1/x^3$ for y = const.

Potential eddy (eq. 33b): $v \sim 1/x$, for y = const.

With regard to the boundary layer expansion and the technical effort, one must try not to build the adaptable measurement lane wall any longer than absolutely necessary.

Figure 10 presents the example of incomplete adaptation for a single potential eddy ($c_A = 0.8$). The example is based on the same calculation as Fig. 7, with the difference that the (freely selected) integration beginning was set at $x_e/L = -2$, and for $x < x_e$ no adaptation was performed. The consequences are jumps in the velocity distribution and a bend in the wall contour. Correspondingly, Fig. 11 shows the overlap of a potential eddy and a dipole.

In order to obtain a quantitative statement about the errors caused by only partial adaptation of a measurement lane, the wall induced interference velocity for the arrangement illustrated in Fig. 10, will be computed approximately, for the tunnel axis.

The calculation is based on the assumption that the compression effect of the model is negligible and the model's effect can be represented by a single potential eddy.

Thus, in a measurement lane arrangement per Fig. 10 we have:

a) In the region $-\infty < x < x_e$ the measurement lane walls are straight and we obtain the velocity distribution by summing an eddy series per eq. (35) (expanded for compressible flow fields via Gothert's rule per eq. (4)):

(36a) $$u_o = \frac{c_A}{2\beta^2 \frac{H}{L}} \frac{1}{2\beta \cosh(\frac{\pi}{\beta}\frac{x}{H})}$$

(36b) $$v_o = 0 .$$

b) In the region $x_e < x < \infty$ complete adaptation of the walls is assumed, and we obtain the velocity distribution from the single eddy per eq. (33):

(37a) $$u_o = \frac{c_A}{2\beta^2 \frac{H}{L}} \frac{1}{\pi\beta[1+(\frac{2x}{\beta H})^2]}$$

(37b) $$v_o = \frac{c_A}{2\beta^2 \frac{H}{L}} \frac{2\frac{x}{H}}{\pi\beta[1+(\frac{2x}{\beta H})^2]} .$$

At the lower wall we have:

(38a) $$u_u = -u_o$$

(38b) $$v_u = v_o .$$

By application of the Cauchy integral formula eq. (13), the wall induced interference velocities at the measurement lane axis (y = 0) can be computed at this wall velocity.

Because of eq. (38), the x-component of the interference velocity disappears: $u_m^i \equiv 0$.

The y-component is plotted in Fig. 12 for various values of x_e as a function of x/L (Ma = 0). We see that the maximum of interference velocity shifts with x_e/L. Since the jump in the velocity distribution increases with approach to the model location, accordingly the maximum of interference velocity also increases.

A much greater interference velocity is seen in Fig. 13, which shows a plot for Ma = 0.85.

The interference velocity and the derivitives of the interference velocity at the measurement site are important for the influence on a wind tunnel measurement in an incompletely adapted measurement lane. The boundary values attained in practice are found in [9]:

$$[v_m^i]_{x=0} < 0{,}01^\circ$$

$$\left[\frac{d\, v_m^i}{d(\frac{x}{L})}\right]_{x=0} < 0{,}03^\circ .$$

The measurement lane lengths necessary to maintain these limit values can be determined with the described calculation method. To do so, compute the lines of equal "interference velocity in the model site" and plot them in Fig. 14. We see that exceptionally large adaptable measurement lane lengths are needed to maintain the specified bounds.

Again in Fig. 14, the lines of equal "gradient error in the model site" are entered. Compared with the lines of equal

interference velocity, much smaller adaptable measurement lane lengths are needed to maintain its limit values.

Whereas a constant interference velocity can be taken into account in the region of the model by a subsequent correction in the angle of attack, a gradient error (i.e. flow line curvature) cannot be corrected. In practice this means that the gradient conditions per Fig. 14 must definately be maintained, whereas a somewhat larger than allowed interference velocity can be accepted in subsequent correction.

But if the presently used adaptable measurement lane is considered (see below), then one comes to the conclusion that all are too short. This leads to considerable measurement errors, especially in the range of larger Mach numbers.

5.2 Turning the Measurement Lane

It was shown that to avoid unacceptable measuring errors, the measurement lane must be adapted to long lengths. Since also the wall boundary layer increases, a very long measurement lane is not necessarily an advantage.

But a bend in the wall contour (Fig. 10 and 11) is completely unsuitable for wind tunnel measurement lanes. Therefore, in completed measurement lanes, an arbitrary transition arc is always inserted in the transition from the fixed to the adapted wall.

A very short and almost disturbance-free measurement lane inlet can be developed by turning the adapted wall so that at point x_e/L the tangent slope of the adapted wall becomes zero:

$$(v^i)_{x=x_e} = 0.$$

We then obtain a bend-free transition between the inlet and the adapted wall, and thus a significant reduction in interferences from non-adapted inlet to the model. However, one must note that the effective angle of attack of the model must be corrected by the rotation angle.

This process is shown in Fig. 15 for a single potential eddy ($c_A = 0.8$). In this example, the angle of rotation is: $\Delta\alpha_e = 0{,}88°$.

Since the rotation applies for the entire adaptable portion of the measurement lane, the outlet angle increases by the same angle. The measurement lane rotation is shown in Fig. 16 for a body with lift and compression ($c_A = 0.8$, R/L = 0.1).

Improvement of flow at the model site can best be shown by performing the same flow calculation as above for Fig. 12 or 13. The result of this calculation is shown in Fig. 17 (Ma = 0) and Fig. 18 (Ma = 0.85).

A comparison of Fig. 12 and 17 (Ma = 0), or of Fig. 13 and 18 (Ma = 0.85), respectively, convincingly demonstrates the attained improvement.

6. Post-Calculation of Wall Induced Flow Velocities at Berlin

6.1 Measurement Program

In the transsonic wind tunnel of the Technical University (TU) of Berlin, systematic measurements were performed with the supercritical profile CAST 7/DoA1 in a two-dimensional adaptive measurement lane and the results are presented in [10].

To check the computation method derived above, several artibrarily selected measurement points were taken from the extensive measurement program and checked.

The geometry of the measurement lane and of the model are specified as follows:

-profile depth: L = 100

-measurement lane width B = 150 mm
(span of the model)

-measurement lane height: H = 150 mm

-length of adaptable part 690 mm

-spindle number (top & bottom) 8 each

-The flexible walls are securely attached to the inflow side

-The flexible walls are securely attached to the outflow side with a small longitudinal mobility.

The adaptation of the measurement lane took place iteratively by the method described by Ganzer [11].

The influence of the boundary layer compression thickness was not taken into account.

The lists of measurements for the last iteration step contain the pressure distribution on the profile, and also the pressure distribution at the adapted wall, as well as the contour of the adapted wall. With this data it is possible to compute the wall induced interference velocity with the Cauchy integral formula.

The computed interference velocity provides information about the residual error affecting the measured results, and also a new,

improved wall contour, which could be used to achieve an interference-free flow.

For the post-calculation, an angle of attack series (polar) was selected at $Ma_\infty = 0.6$ (Figs. 19 to 24) and a Mach number series at $\alpha = 0.81^o$ (Figs. 25 to 28).

The figures all have the same structure and are plotted against the tunnel axis.

a) Top: The u and v-components of the wall induced interference velocity on the tunnel axis.
b) Middle: Given contour and computed interference-free contour for the upper and lower wall.
c) Bottom: Measured and computed interference velocity for interference-free flow at the upper and lower walls.

6.2 Residual Correction

To determine the residual corrections, every interference velocity distribution in the range $0 \leq x \leq L$ was approximated by an equalization line. Thus, only error influences up to 1st order were considered. The figures do show however, that the equalization line does not always exactly reproduce the curve profile.

The equalization line can be broken down into a constant portion:

$$\Delta Ma_\infty/Ma_\infty = u_m^i, \quad \text{for } x/L = 0.50$$

$$\Delta \alpha \quad = v_m^i, \quad \text{for } x/L = 0.50$$

and a gradient:

$$\frac{d\left(\frac{\Delta Ma_\infty}{Ma_\infty}\right)}{d\left(\frac{x}{L}\right)} = \frac{du_m^i}{d\left(\frac{x}{L}\right)}, \quad \text{for } x/L = 0.50$$

$$\frac{d(\alpha)}{d\left(\frac{x}{L}\right)} = \frac{dv_m^i}{d\left(\frac{x}{L}\right)}, \quad \text{for } x/L = 0.50.$$

The constant portion is the Mach number correction or angle of attack correction, and is simply applied to the measured results. The gradient of the compensation lines is an acceleration or parabolic curvature of flow lines (2nd Birnbaum normal distribution) and is generally not correctable.

The residual corrections for the post-calculated examples were summarized in Table 1 and compared with those values taken from [9].

In considering the uncorrectable errors, the very large curvature corrections at large angles of attack and high Mach numbers are particularly striking.

6.3 Improving the Wall Contour

Like the simple singularity arrangements, the wall-induced interference velocity was computed at the location of the wall and from this, the improved velocity distribution and wall contour were determined.

For the calculations, the given wall contour points were linked by a spline function and the given velocity distribution was linked by linear interpolation.

The reason for the different interpolations is that the wall contour is physically also a bending line, whereas the wall pressures scatter and a non-linear interpolation easily leads to undesirable overshoots.

A comparison of given and improved wall contour gives a good indication of possible sources of error:

-The compression influence of the model has not decayed sufficiently at the measurement lane inlet (example: Fig. 19)

-Since the wall contour at the inlet must follow the bending line of the fixed beam, the correct wall contour is not adjustable. This is noticed particularly for large angles of attack (example: Fig. 24).

-Reconversion of the wall shape to the inflow direction takes place shortly behind the model. This causes significant interference velocities (example: Fig. 24).

-The total pressure loss in the measurement lane due to wall friction and model resistance causes a Mach number gradient if the outlet cross-section is no greater than the inlet cross-section.

-At large Ma numbers the wall induced interference velocity (u-component) in the region of the model is also still very large after the adaptation. It could possibly be avoided by taking into account the boundary layer compression thickness (example: Fig. 28).

Since it is not entirely certain whether the boundary conditions used in the calculation represent the test arrangement

in all details, the calculated results also contain a certain uncertainty. A final error estimation should thus be performed only after a more accurate examination.

7. Post-Calculation of Wall Induced Interference Velocities in Toulouse

7.1 Measurement Program

Other detailed experimental investigations with the supercritical profile CAST 7/DoA1 were performed in the adaptive measurement lane of the transsonic wind tunnel T2 of ONERA/CERT in Toulouse [12]. The geometry of the measurement lane and of the model are specified as follows:

-profile depth: L = 200 mm

-measurement lane width B = 390 mm

(span of the model)

-measurement lane height H = 370 mm

-length of adaptable part: 1320 mm

-number of spindles (top & bottom) 16 each

-The flex. walls are securely stretched at the inflow side

-The walls on the outflow side are not attached and can move freely.

Adaptation of the measurement lane takes place by an iterative method of Chevallier [13].

The influence of the boundary layer was taken into account inasmuch as the boundary layer was computed for all four walls and the combined compressive thickness was subtracted from the upper and lower wall contour. For the resulting boundary of frictionless flow, the improved contour was determined by the method of Chevallier, and by adding the boundary layer compressive thickness, an (improved) physical contour was then obtained.

The lists of results [12] provide both the physical contour as well as the contour of frictionless flow for all iteration steps. The following calculations and comparisons pertain to this frictionless contour alone. Both the residual correction and the improved wall contour are computed for all iteration steps of several selected measured points (Figs. 29 to 44).

7.2 Residual Correction

The residual corrections for the post-calculated points are presented in Table 2 and the characteristic curves are in Figures 29 to 44. Like the measurements at the TU Berlin, the very strict requirements presented in [9] are sometimes greatly exceeded.

Since each iteration proceeds from a preconception obtained by estimation, sometimes only slight improvements are possible. In none of the post-calculated measurements is a smooth decrease of all residual corrections observed, i.e. the adaptation process probably does not converge.

In measurements no. 370 and 376, a decrease in the residual corrections is observed, but very many iteration steps would be required to reach the range of permissible residual corrections.

The reason for the unsatisfactory convergence cannot be investigated at this point. But one could suppose that it is connected with the boundary layer correction method.

7.3 Improving the Wall Contour

By computing the wall-induced interference velocity at the point of the wall, we obtain, as stated above, the improved velocity distribution and the improved wall contour.

For these calculations, the given points of the "frictionless contour" were linked by a spline function, and the given velocity distribution by a linear interpolation. In a comparison of given and improved wall contour, the following observations need to be stressed:

-The compression influence of the modes has not decayed sufficiently at the measurement lane inlet (example: Figs. 38 to 41).

-The evaluated examples well confirm that the computation method used here is a one-step method; the same contour and the same velocity distribution were determined for each iteration step.

-The intersection of the improved wall contour (example: Figs. 34 to 37) cannot be correct, for physical reasons. An explanation of this phenomenon might reside in the boundary layer correction method.

In summary, we find that the advantages of the new computation method in post-calculation of the interation steps are quite evident.

8. Post-Calculation of Wall Induced Flow Velocity by ONERA

8.1 Measurement Program

Additional measurements within the framework of the GARTEur-program "Two-Dimensional Transsonic Testing Methods" (Action Group 02) were performed with the profile CAST 7/DoA1 in the ONERA S3 MA wind tunnel in Modane [14]. Some of these measurements were taken in the enclosed measurement lane of this wind tunnel. Several points of these measurements were post-calculated.

The geometry of the measurement lane and of the model are specified as follows:

-profile depth: L = 200 mm

-measurement lane width B = 560 mm
(span of the model)

-measurement lane height H = 780 mm

The measurement lane walls are closed. A boundary layer calculation was not performed, but the pressure distribution in the empty measurement lane was taken into account. From the corrected wall pressure distribution, both the residual corrections at the side of the model, and also the interference-free wall flow line were computed by using the Cauchy integral formula, as for the other examples. Since the walls of the used wind tunnel are not adaptable and an adaptation is not even intended,

these results are without practical significance. The measurement and computed results are presented in Figs. 45 to 49. The structure of these diagrams is just as described in Section 6.1.

8.2 Residual Corrections

As described in Section 6.2, the interference velocity distribution was approximated by an equalization line on the measurement lane axis in the range of $0 \leq x \leq L$, to determine the residual corrections.

The constant portions of the residual corrections are defined differently from the measurements described above:

$$\Delta Ma_\infty/Ma_\infty = u_m^i, \quad \text{at } x/L = 0.25$$

$$\Delta \alpha = v_m^i, \quad \text{at } x/L = 0.75.$$

The residual corrections for the post-calculated examples are presented in Table 4. For comparison, the permissible values taken from [9] are also entered. Moreover, the corrections given in [14] for the constant portion, are also entered in the tables.

It turns out that the residual corrections are not very large, in spite of the enclosed, straight walls. This is attributable to the relatively great height of the measurement lane.

Moreover, the Mach number corrections of ONERA and of the DFVLR show good agreement.

The ONERA corrections to the angle of attack are greater than those computed by the DFVLR and also point in the opposite direction.

9. Summary

From the Cauchy integral formula a method was derived for direct calculation of the wall induced interference velocity in a two-dimensional frictionless flow. With this "one step method", the interference velocity generated by the measurement lane wall can be determined at each point of the flow field and at the site of the wall, solely from the wall pressure distribution and the wall contour (without model representation). Computation formulas were derived both for infinite and also for finite long measurement lanes.

Application of the method was illustrated on simple, singularity arrangements (dipole, potential eddy). It turned out that for a good adaptation, considerable measurement lane lengths are needed. The error due to incomplete adaptation (too short a lane) was estimated and in addition, a method was given to reduce the residual error considerably, by rotating the model together with the adaptable part of the measurement lane.

Since detailed, documented measurements, including wall pressure distributions are available from the GARTEur program "Two-Dimensional testing Methods" using the CAST 7 profile in the following wind tunnels:

-transsonic wind tunnel of the TU Berlin

-T2 of ONERA, Toulouse

-S3 of ONERA, Modane,

it was possible to make practical testing of the computation method. The results give important indications for refinement of

the method (taking the boundary layer into account) and for structuring the adaptable measurement lanes.

10. References

[1] Mokry, M., Chan, Y.Y., Jones, D.J.: Two-Dimensional Wind-Tunnel Wall Interference. AGARDograph No. 281 (1983).

[2] Hurwitz, A., Courant, R.: General Function Theory and Elliptical Functions. Berlin, Goettingen, Heidelberg, New York: Springer-Pub. 1964.

[3] Aerodynamic Theory, Vol. I. Ed. W.F. Durand. Berlin: Julius Springer, 1934.

[4] Smith, J.: A Method for Determining 2-D Wall Interference on an Aerofoil from Measured Pressure Distributions near the Walls and on the Model. NLR TR 81016 U (1981).

[5] Goethert, B.: Planar and Spatial Flow at High Subsonic Speeds. Jahrb. dt. Lufo 1941, p. I 156-158.

[6] Schlichting, H., Truckenbrodt, E.: Aerodynamics of the Airplane, Volume One. Berlin, Goettingen, Heidelberg: Springer Pub., 1959.

[7] Knopp, K.: Theory and Application of Infinite Series. Berlin, Goettingen, Heidelberg, New York: Springer Publ, 1964.

[8] Groebner, W., Hofreiter, N.: Integral Table. Vienna, Innsbruck: Springer Pub., 1957.

[9] Steinle, F., Stanewsky, E.: Wind Tunnel Flow Quality and Data Accuracy Requirements. AGARD-AR-184 (1982).

[10] Ziemann, J.: Data Report on the CAST7/DOA1 Aerofoil in the TU Berlin Transsonic Wind Tunnel. ILR Mitt. 94 (1981).

[11] Ganzer, U.: Wind Tunnels with Adaptive Walls to Eliminate Wall Interferences. Z. Flugwiss. Weltraumforsch. 3 (1979), p. 129-133.

[12] Archambaud, J.P., Mignosi, A., Seraudie, A.: Rapport d'essais sur profil CAST 7 effectues a la soufflerie T2 en presence de parois auto-adaptables en liaison avec le group GARTEUR AD (AG 02). Rapp. Techn. OA No. 24/3075 AND (1982).

[13] Chevallier, J.P., Mignosi, A., Archambaud, J.P., Seraudie, A.: T2 Wind Tunnel Adaptive Walls: Design, Construction and some Typical Results. Rech. Aerosp. 1983-4 (1983).

[14] Vaucheret, X.: Data Report on the CAST7/DoA1 Profile in the ONERA S3MA Wind Tunnel. ONERA Techn. Rep. No. 201/1464 GN (1982).

List of Tables

List of Illustrations

Fig. 32: Measurement Point Ma = 0.81 and alpha = 0.0 (4th Iteration) by T2 Toulouse

Fig. 33: Measurement Point Ma = 0.81 and alpha = 0.0 (5th Iteration) by T2 Toulouse

Fig. 34: Measurement Point Ma = 0.60 and alpha = 4.0 (1st Iteration) by T2 Toulouse

Fig. 35: Measurement Point Ma = 0.60 and alpha = 4.0 (2nd Iteration) by T2 Toulouse

Fig. 36: Measurement Point Ma = 0.60 and alpha = 4.0 (3rd Iteration) by T2 Toulouse

Fig. 37: Measurement Point Ma = 0.60 and alpha = 4.0 (4th Iteration) by T2 Toulouse

Fig. 38: Measurement Point Ma = 0.75 and alpha = 3.5 (1st Iteration) by T2 Toulouse

Fig. 39: Measurement Point Ma = 0.75 and alpha = 3.5 (2nd Iteration) by T2 Toulouse

Fig. 40: Measurement Point Ma = 0.75 and alpha = 3.5 (3rd Iteration) by T2 Toulouse

Fig. 41: Measurement Point Ma = 0.75 and alpha = 3.5 (4th Iteration) by T2 Toulouse

Fig. 42: Measurement Point Ma = 0.60 and alpha = 5.0 (1st Iteration) by T2 Toulouse

Fig. 43: Measurement Point Ma = 0.60 and alpha = 5.0 (2nd Iteration) by T2 Toulouse

Fig. 44: Measurement Point Ma = 0.60 and alpha = 5.0 (3rd Iteration) by T2 Toulouse

Fig. 45: Measurement Point Ma = 0.60 and alpha = -2.63 by S3 Modane

Fig. 46: Measurement Point Ma = 0.60 and alpha = -1.75 by S3 Modane

Fig. 47: Measurement Point Ma = 0.60 and alpha = 0.19 by S3 Modane

Fig. 48: Measurement Point Ma = 0.60 and alpha = 1.24 by S3 Modane

Fig. 49: Measurement Point Ma = 0.60 and alpha = 2.28 by S3 Modane

Nr.	Ma_∞	α [°]	c_A	c_W	$\frac{\Delta Ma_\infty}{Ma_\infty}$	$\Delta\alpha$ [°]	$\frac{d(\frac{\Delta Ma_\infty}{Ma_\infty})}{d(\frac{x}{L})}$	$\frac{d(\Delta\alpha)}{d(\frac{x}{L})}$ [°]
1 Zulässige Werte nach [9]					±0,0010	±0,0100	±0,0006	±0,0300
	0,600	-2,00	0,051		0,0081	-0,0622	0,0014	-0,0025
	0,600	-1,00	0,182		0,0075	-0,0322	0,0016	0,0110
	0,600	0,00	0,319		0,0070	-0,0200	0,0015	0,0460
	0,600	4,00	0,822		0,0055	0,0545	0,0014	0,0884
	0,600	6,00	1,065		0,0035	0,0943	0,0018	0,1103
	0,600	8,00	1,058		0,0075	0,0679	0,0015	0,1829
	0,720	0,81	0,482		0,0096	0,0006	0,0013	0,0993
	0,760	0,81	0,520		0,0113	0,0099	0,0005	0,1847
	0,800	0,81	0,500		0,0150	-0,0037	0,0010	0,2574
	0,820	0,81	0,416		0,0174	-0,0028	-0,0002	0,2845

Table 1: Residual Correction of Post-Calculated Measurement Points by the TU, Berlin

Key: 1-permissible values per [9]

Nr.	Ma_∞	α [°]	c_A	c_W	$\frac{\Delta Ma_\infty}{Ma_\infty}$	$\Delta\alpha$ [°]	$\frac{d(\frac{\Delta Ma_\infty}{Ma_\infty})}{d(\frac{x}{L})}$	$\frac{d(\Delta\alpha)}{d(\frac{x}{L})}$ [°]
1 Zulässige Werte nach [9]					±0,0010	±0,0100	±0,0006	±0,0300
340/1	0,813	0,00			0,0090	-0,0094	0,0005	-0,0285
340/2	0,815	0,00			0,0001	0,0326	-0,0010	0,1710
340/3	0,814	0,00			0,0059	0,0099	0,0003	0,0076
340/4	0,815	0,00			0,0007	0,0148	-0,0003	0,1396
340/5	0,814	0,00	0,405	0,026	0,0058	0,0113	0,0002	0,0348
370/1	0,602	4,00			-0,0067	0,1414	0,0023	0,5022
370/2	0,602	4,00			-0,0058	0,0116	0,0018	0,2584
370/3	0,602	4,00			-0,0044	0,0311	0,0012	0,2149
370/4	0,602	4,00	0,983	0,015	-0,0049	0,0230	0,0009	0,1733
374/1	0,754	3,50			0,0117	0,0739	0,0065	0,1801
374/2	0,755	3,50			0,0016	0,0363	0,0026	0,2329
374/3	0,754	3,50			0,0049	0,0317	0,0020	0,1971
374/4	0,754	3,50	0,801	0,067	0,0038	0,0238	0,0018	0,2105
376/1	0,601	5,00			-0,0049	0,0302	0,0013	0,2210
376/2	0,602	5,00			-0,0048	0,0216	0,0011	0,2251
376/3	0,601	5,00	1,112	0,024	-0,0028	0,0246	0,0010	0,2023

Table 2: Residual Correction of Post-Calculated Measurement Points by T2, Toulouse

Key: 1-permissible values per [9]

1 Nr.	Ma_∞	α [°]	c_A	c_W	$\frac{\Delta Ma_\infty}{Ma_\infty}$	$\Delta\alpha$ [°]	$\frac{\Delta Ma_\infty}{d(\frac{Ma_\infty}{Ma_\infty})}$	$\frac{d(\Delta\alpha)}{d(\frac{x}{L})}$ [°]
2 Zulässige Werte nach [9]					±0,0010	±0,0100	±0,0006	±0,0300
1156	0,596	-2,63	0,024	0,009	0,0068	-0,0831	0,0002	0,0220
1157	0,596	-1,75	0,151	0,009	0,0073	-0,0460	0,0002	0,0984
1159	0,597	0,19	0,427	0,010	0,0080	0,0433	0,0003	0,2631
1160	0,595	1,24	0,572	0,010	0,0073	0,1007	0,0003	0,3482
1175	0,595	2,28	0,722	0,012	0,0102	0,1316	0,0003	0,4430
1156	0,596	-2,63	0,024	0,009	0,0065	-0,2000	3 Rechnung ONERA	
1157	0,596	-1,75	0,151	0,009	0,0070	-0,2300		
1159	0,597	0,19	0,427	0,010	0,0081	-0,2700		
1160	0,595	1,24	0,572	0,010	0,0078	-0,2600		
1175	0,595	2,28	0,722	0,012	0,0116	-0,3400		

Table 3: Residual Correction of Post-Calculated Measurement Points by S3, Modane

Key: 1-no. 2-permissible values per [9] 3-ONERA calculation

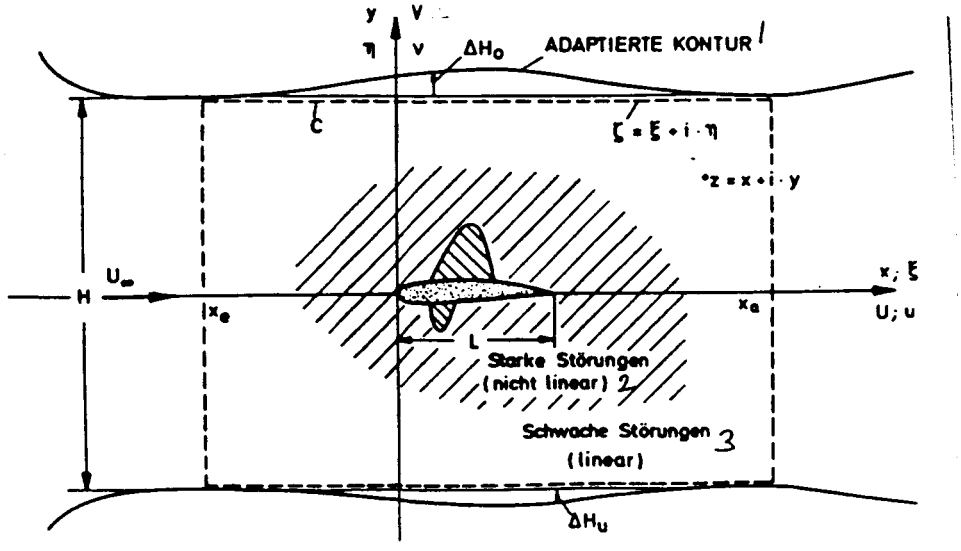

Fig. 1: Definitions

Key: 1-adapted contour 2-severe turbulance (non-linear) 3-weak turbulance (linear)

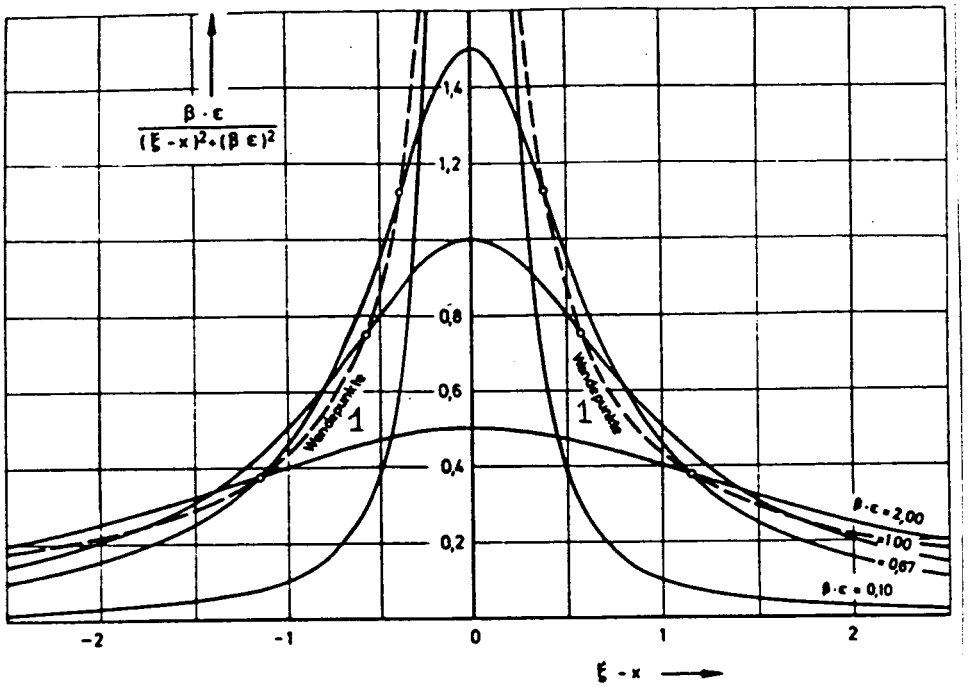

Fig. 2: Integrand of Eq. (19)

Key: 1-inflection points

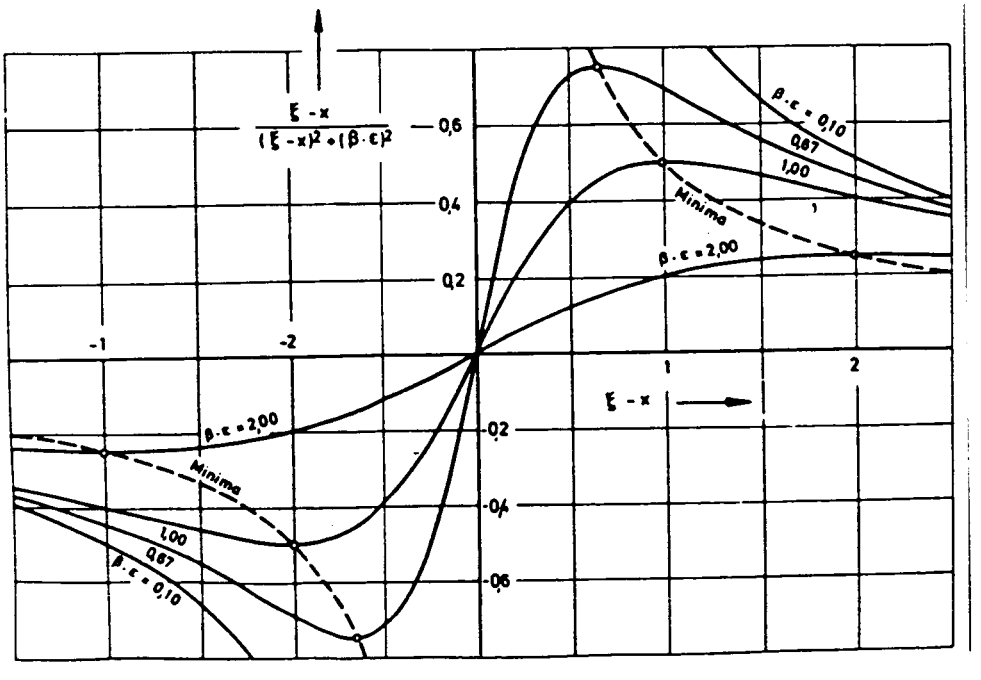

Fig. 3: Integrand of Eq. (22)

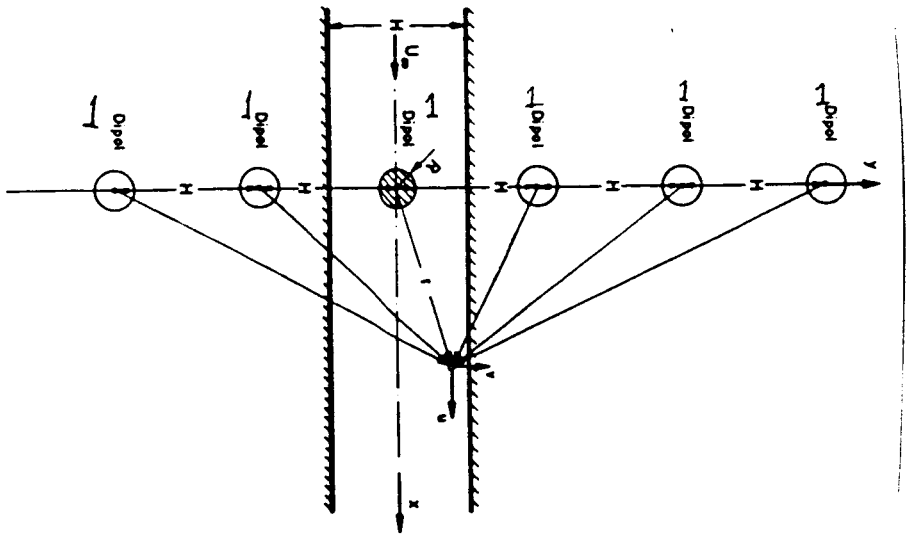

Fig. 4: Dipole (Circular Cylinder) in a Planar Measurement Lane

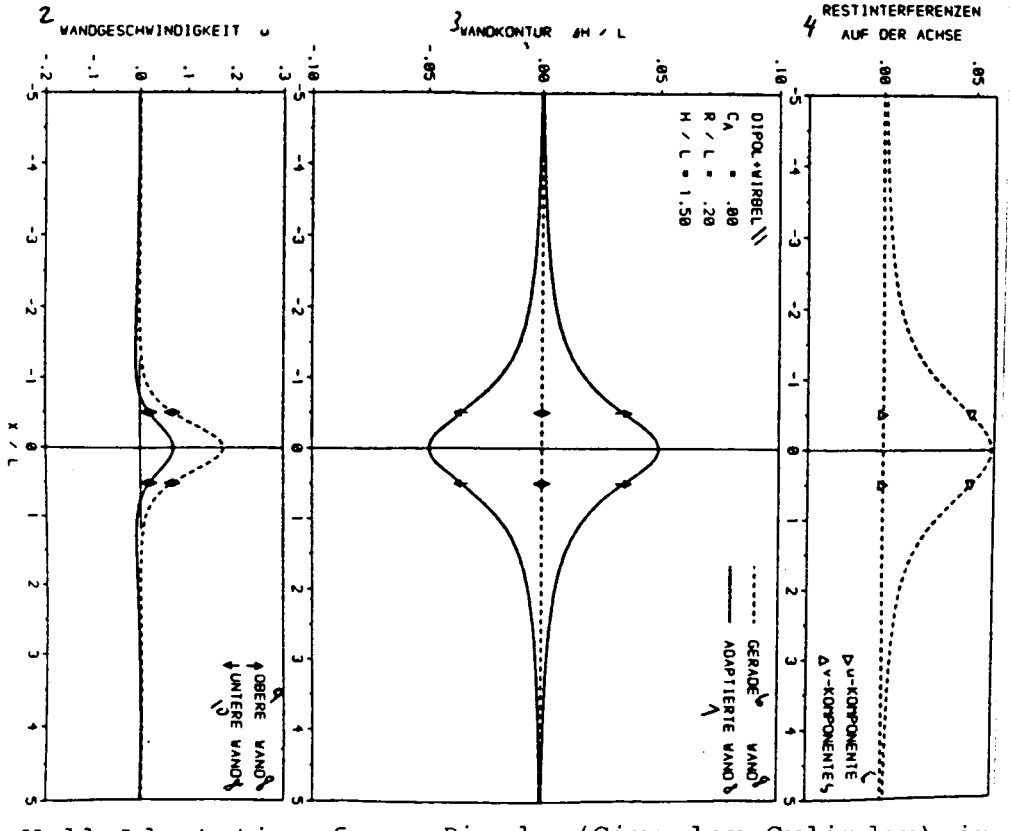

Fig. 5: Wall Adaptation for a Dipole (Circular Cylinder) in a Planar Measurement Lane

Key: 1-dipole 2-wall velocity 3-wall contour 4-residual interferences on the axis 5-component 6-straight 7-adapted 8-wall 9-upper 10-lower 11-dipole + eddy

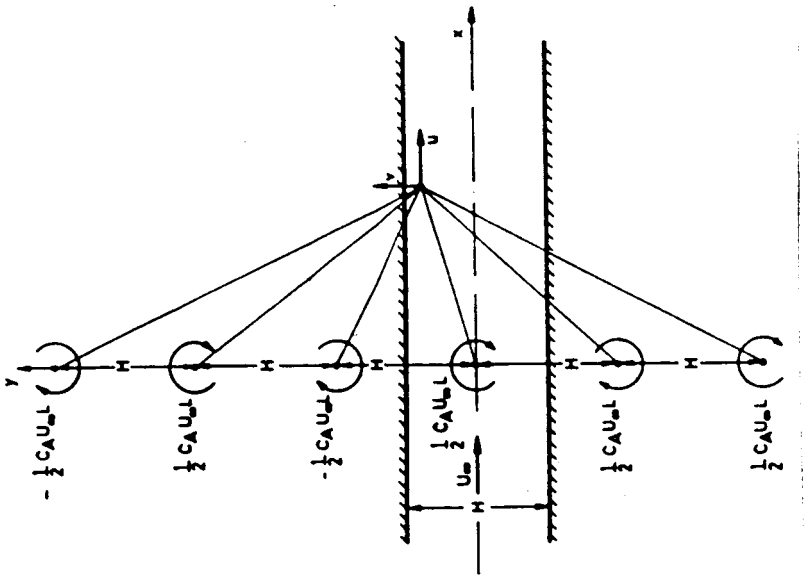

Fig. 6: Potential Eddy in a Planar Measurement Lane

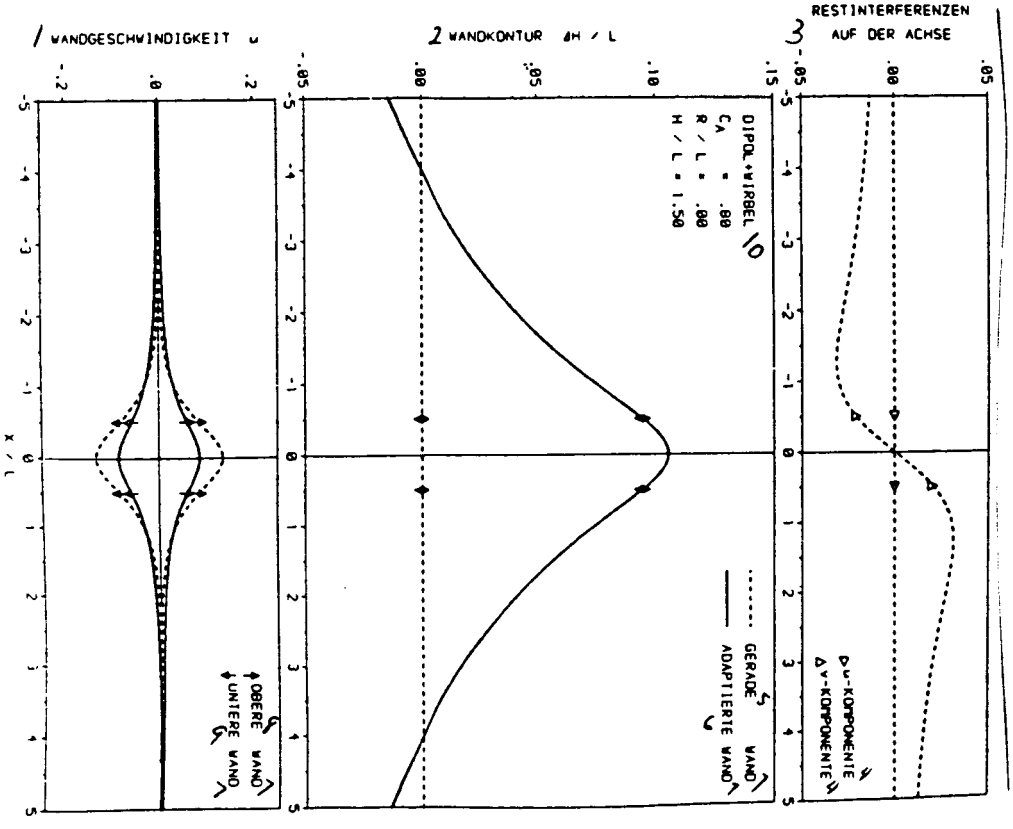

Fig. 7: Wall Adaptation for a Potential Eddy in a Planar Measurement Lane

Key: 1-wall velocity 2-wall contour 3-residual interferences on the axis 4-component 5-straight 6-adapted 7-wall 8-upper 9-lower 10-dipole + eddy

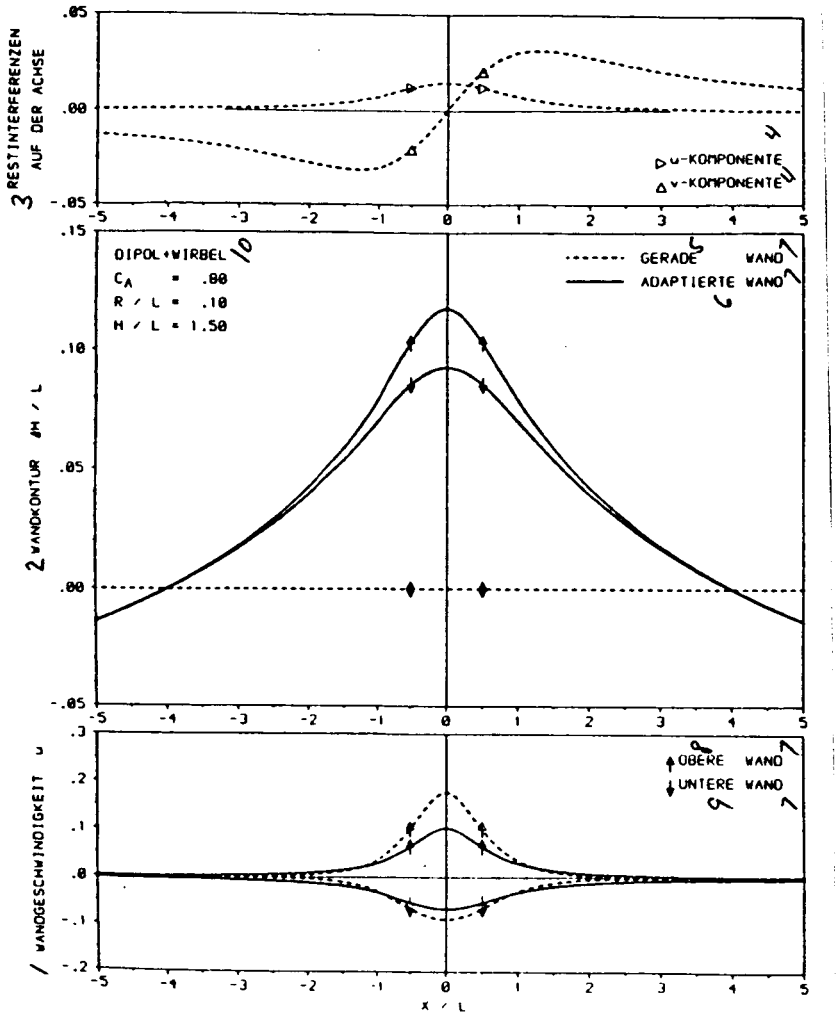

Fig. 8: Wall Adaptation for a Potential Eddy and Dipole (R/L = 0.1)

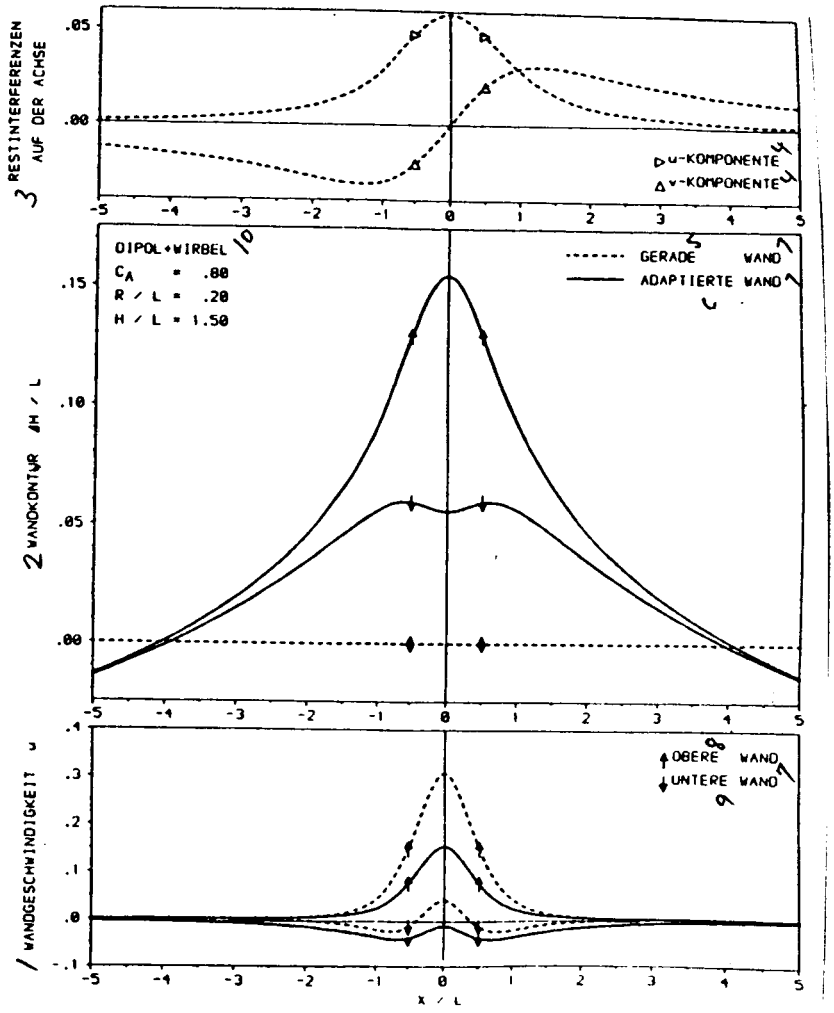

Fig. 9: Wall Adaptation for a Potential Eddy and Dipole (R/L = 0.2)

Key: 1-wall velocity 2-wall contour 3-residual interferences on the axis 4-component 5-straight 6-adapted 7-wall 8-upper 9-lower 10-dipole + eddy

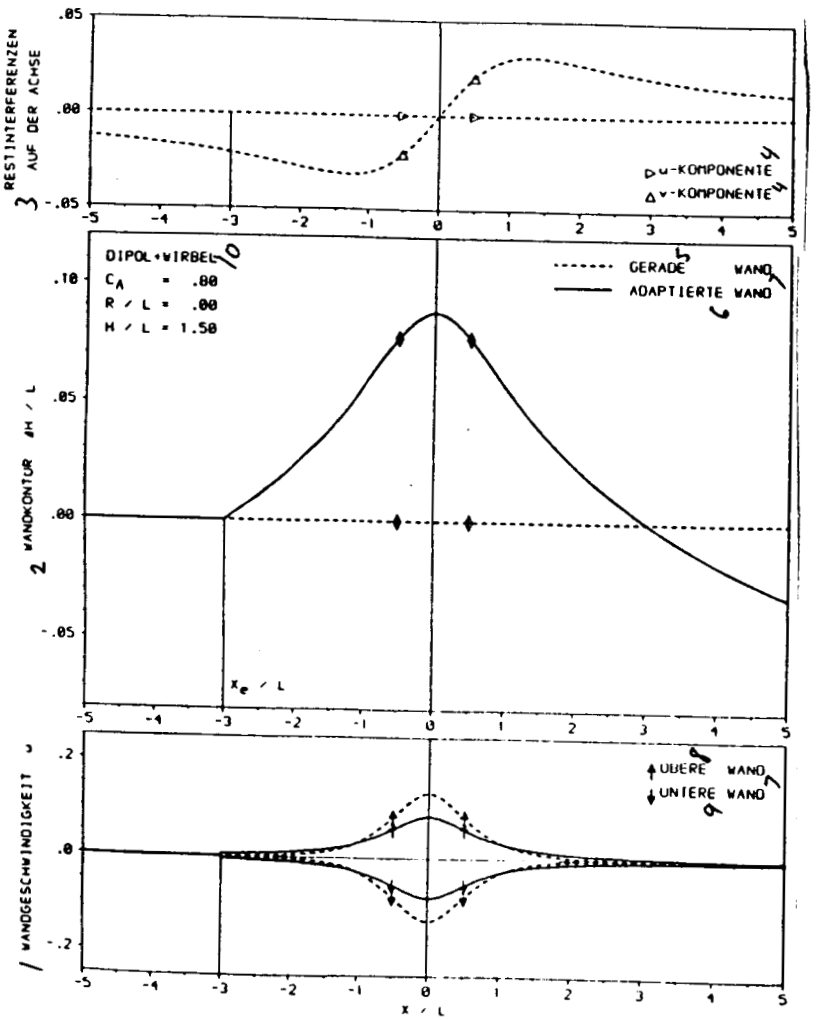

Fig. 10: Incomplete Wall Adaptation for a Potential Eddy

Key: 1-wall velocity 2-wall contour 3-residual interferences on the axis 4-component 5-straight 6-adapted 7-wall 8-upper 9-lower 10-dipole + eddy

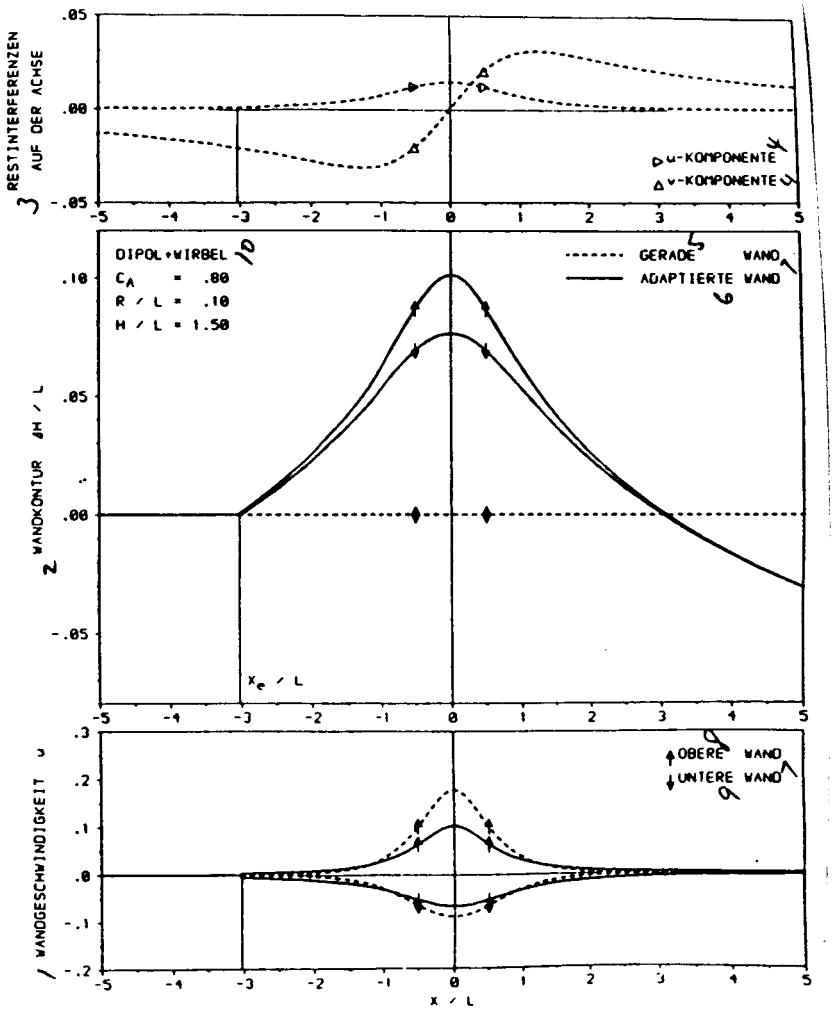

Fig. 11: Incomplete Wall Adaptation for a Potential Eddy and Dipole

Key: 1-wall velocity 2-wall contour 3-residual interferences on the axis 4-component 5-straight 6-adapted 7-wall 8-upper 9-lower 10-dipole + eddy

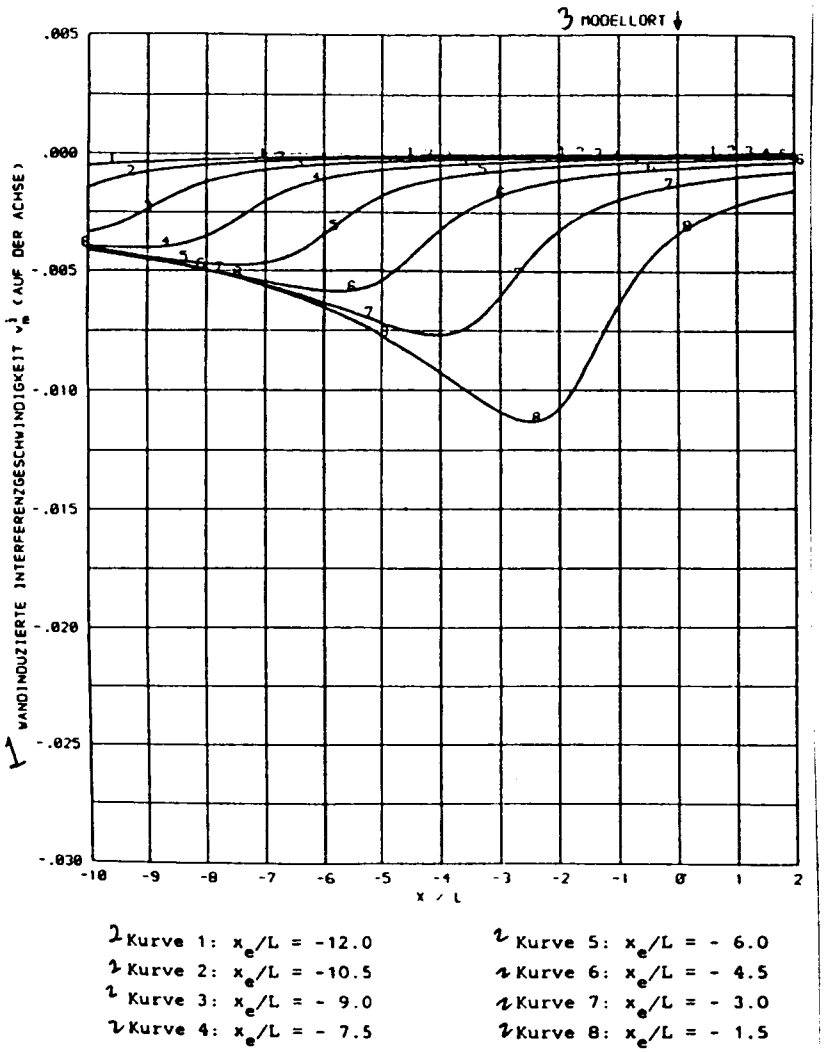

Fig. 12: Residual Interferences for Incomplete Adaptation for Ma = 0 as a Function of the Distance to Measurement Lane Inlet (cA = 0.60 and H/L = 2.00

Key: 1-wall induced interference speed (on the axis) 2-curve 3-model site

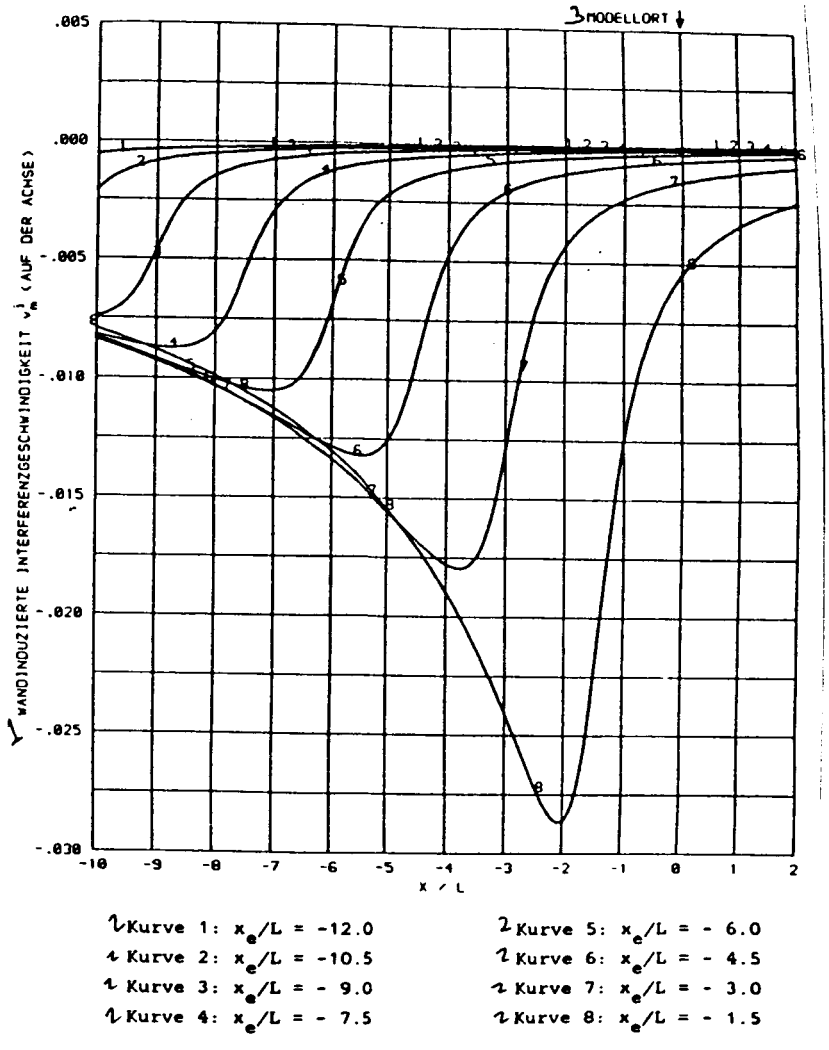

Fig. 13: Residual Interferences for Incomplete Adaptation for Ma = 0.85 as a Function of the Distance to Measurement Lane Inlet (cA = 0.60 and H/L = 2.00)

Key: 1-wall induced interference speed (on the axis) 2-curve 3-model site

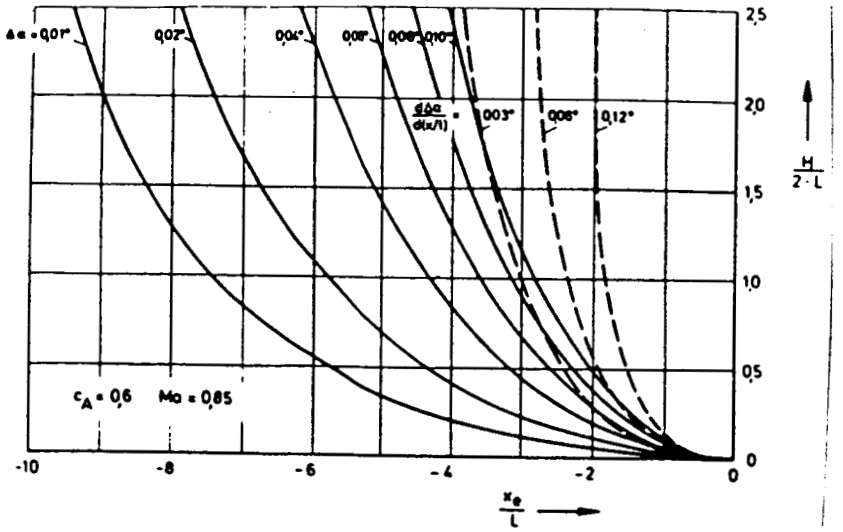

Fig. 14: Residual Interferences at the Model Site for Incomplete Adaptation

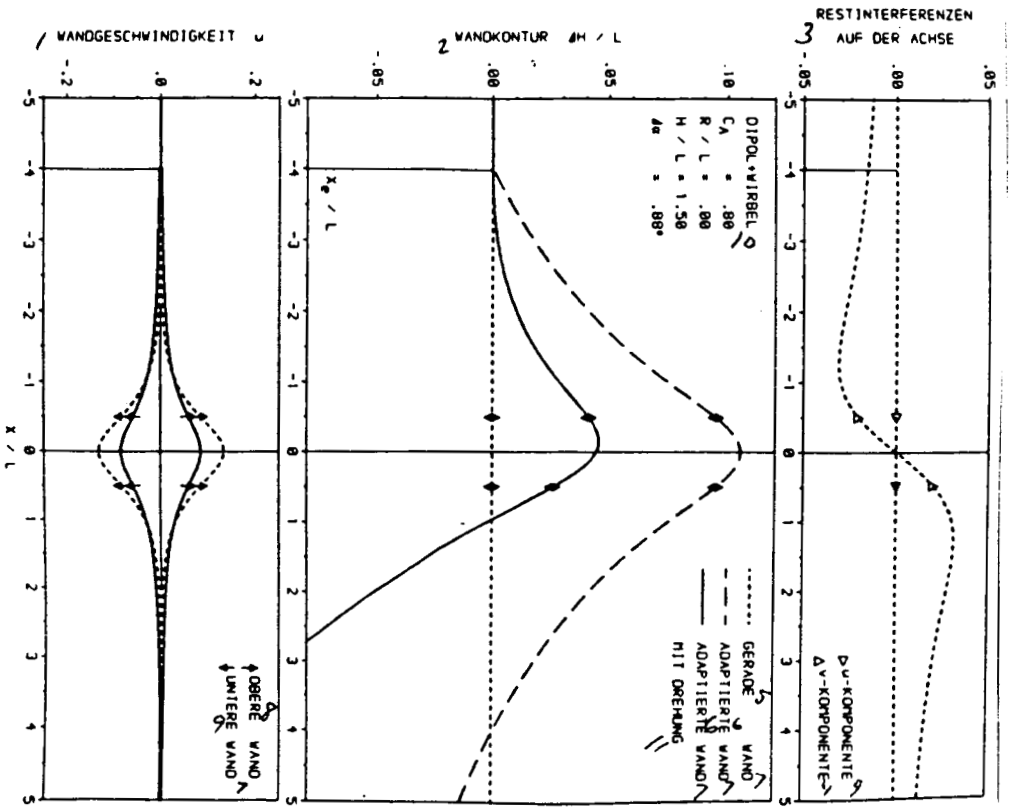

Fig. 15: Wall Adaptation with Rotation of Measurement Lane for a Potential Eddy

Key: 1-wall velocity 2-wall contour 3-residual interferences on the axis 4-component 5-straight 6-adapted 7-wall 8-upper 9-lower 10-dipole + eddy 11-with rotation

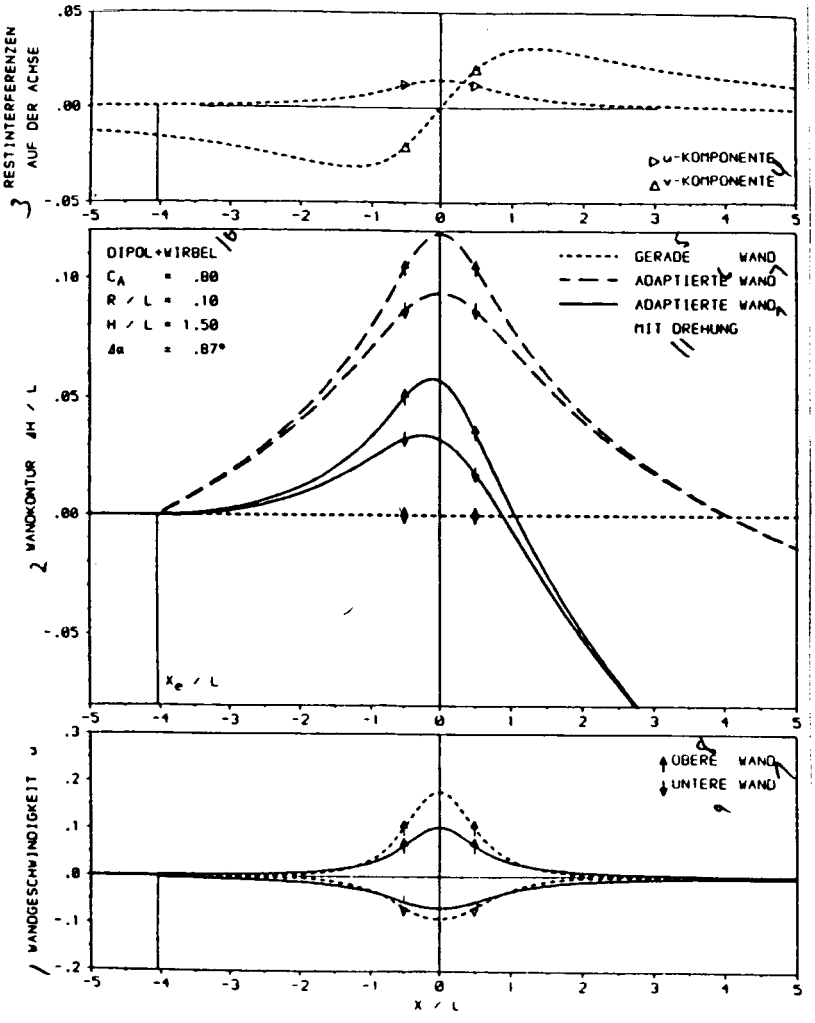

Fig. 16: Wall Adaptation with Rotation of Measurement Lane for a Potential Eddy and Dipole

Key: 1-wall velocity 2-wall contour 3-residual interferences on the axis 4-component 5-straight 6-adapted 7-wall 8-upper 9-lower 10-dipole + eddy 11-with rotation

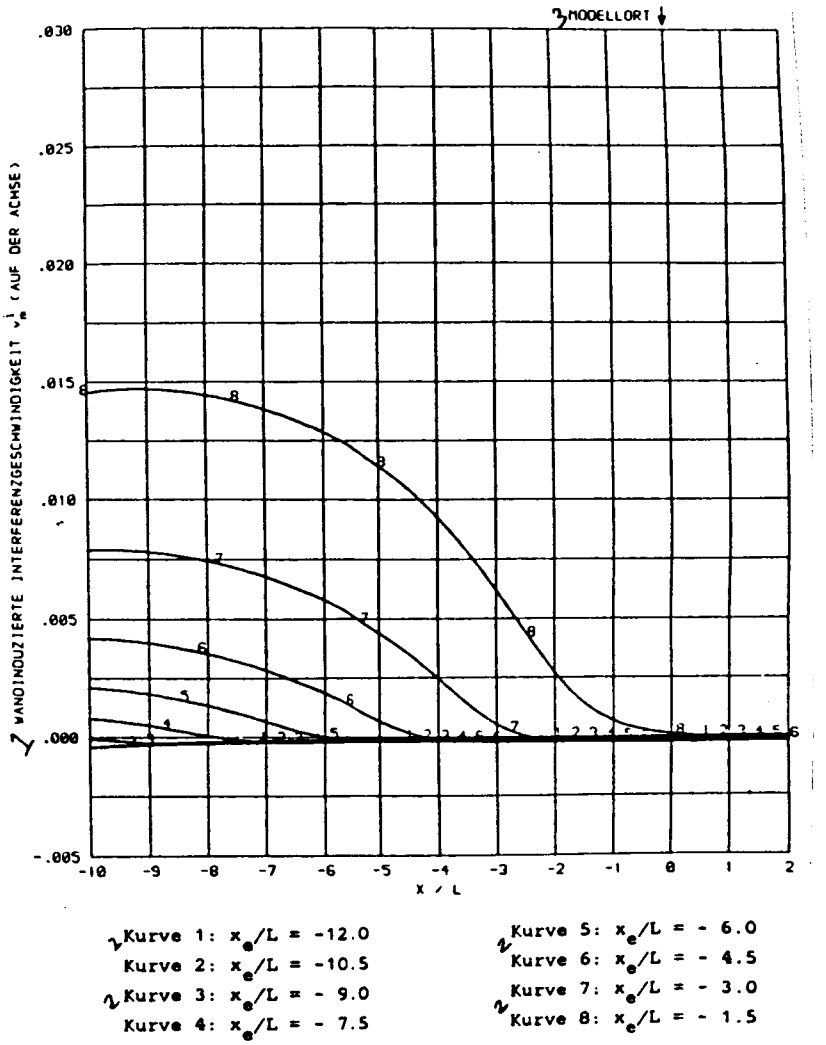

Fig. 17: Residual Interferences with Rotation of Measurement Lane for Ma = 0 as a Function of Distance from Measurement Lane Inlet (cA = 0.60 and H/L = 2.00)

Key: 1-wall induced interference velocity (on the axis) 2-curve 3-model site

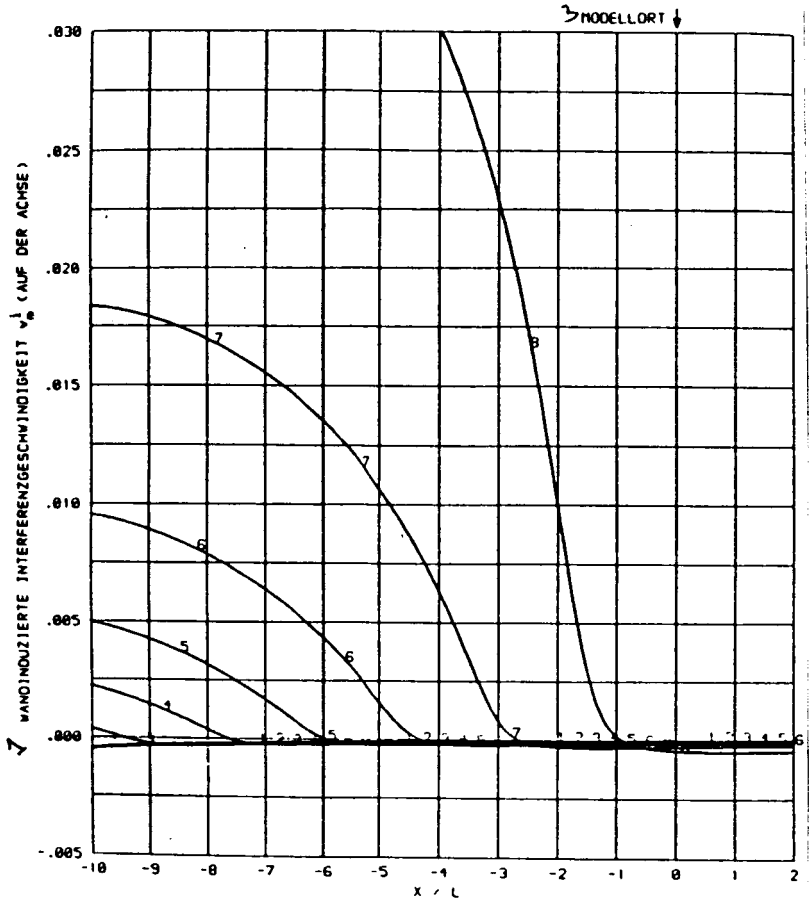

Fig. 18: Residual Interferences with Rotation of Measurement Lane for Ma = 0.85 as a Function of Distance from Measurement Lane Inlet (cA = 0.60 and H/L = 2.00)

Key: 1-wall induced interference velocity (on the axis) 2-curve 3-model site

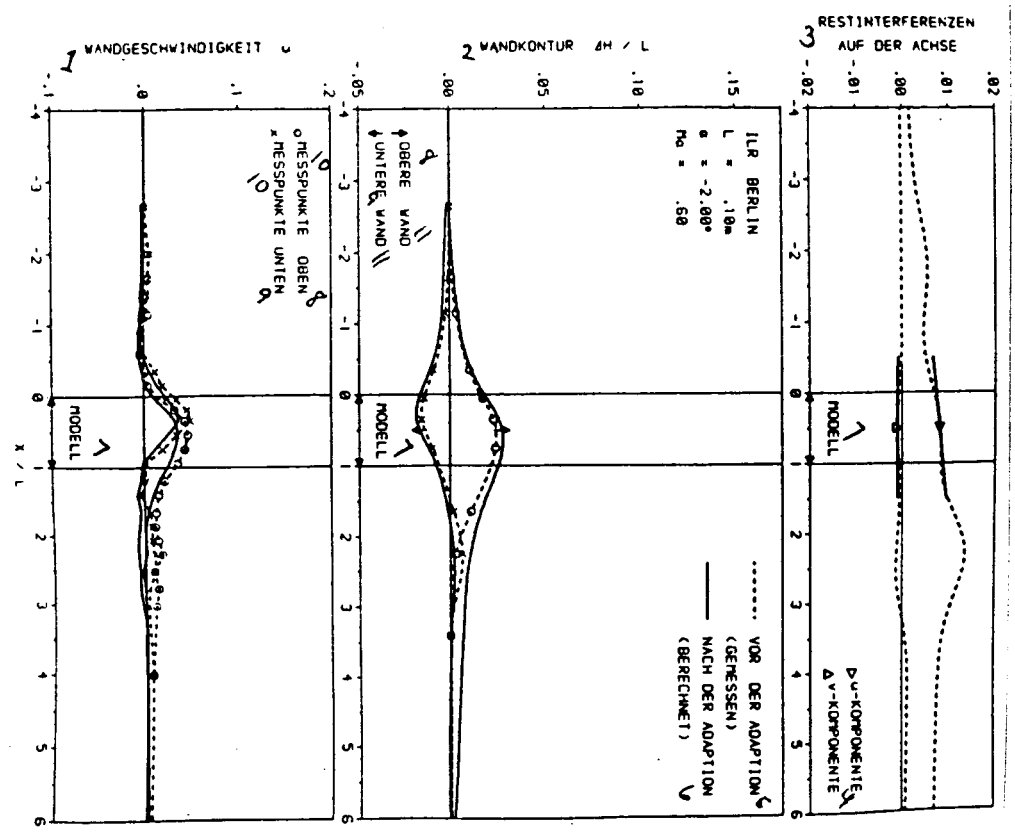

Fig. 19: Measurement Point Ma = 0.60 and alpha = -2.00 by TU Berlin

Key: 1-wall velocity 2-wall contour 3-residual interferences on the axis 4-component 5-before adaptation (measured) 6-after adaptation (calculated) 7-model 8-upper 9-lower 10-measured point 11-wall

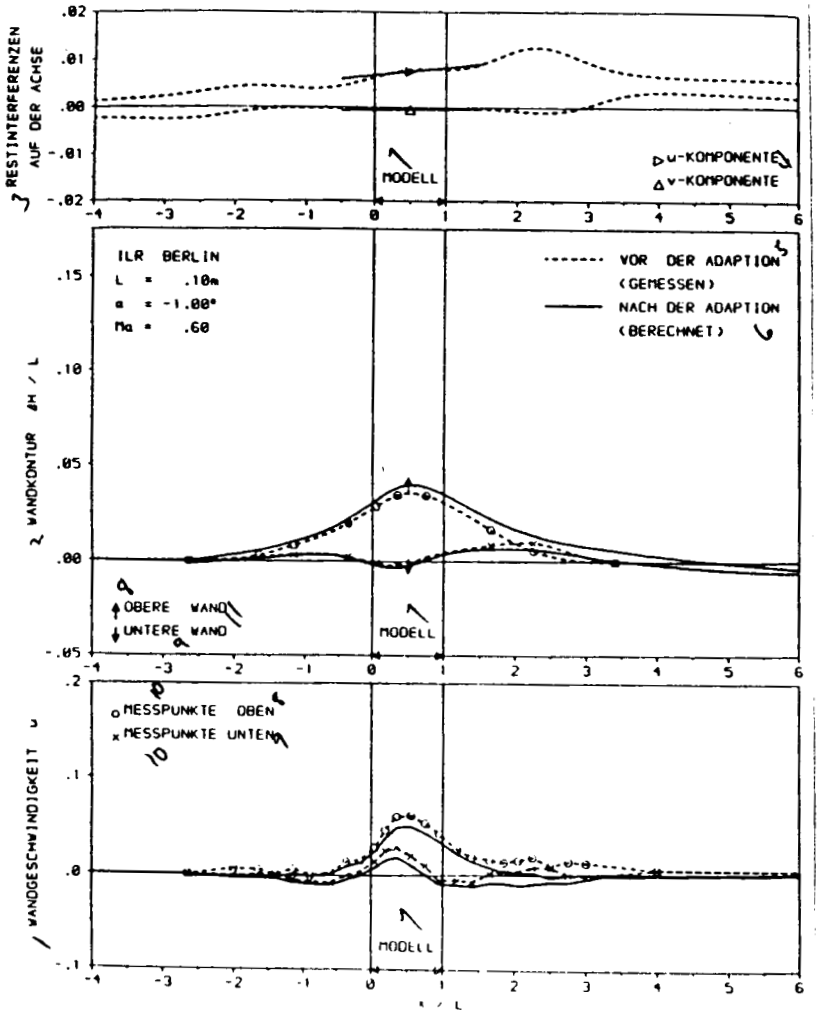

Fig. 20: Measurement Point Ma = 0.60 and alpha = -1.00 by TU Berlin

Key: 1-wall velocity 2-wall contour 3-residual interferences on the axis 4-component 5-before adaptation (measured) 6-after adaptation (calculated) 7-model 8-upper 9-lower 10-measured point 11-wall

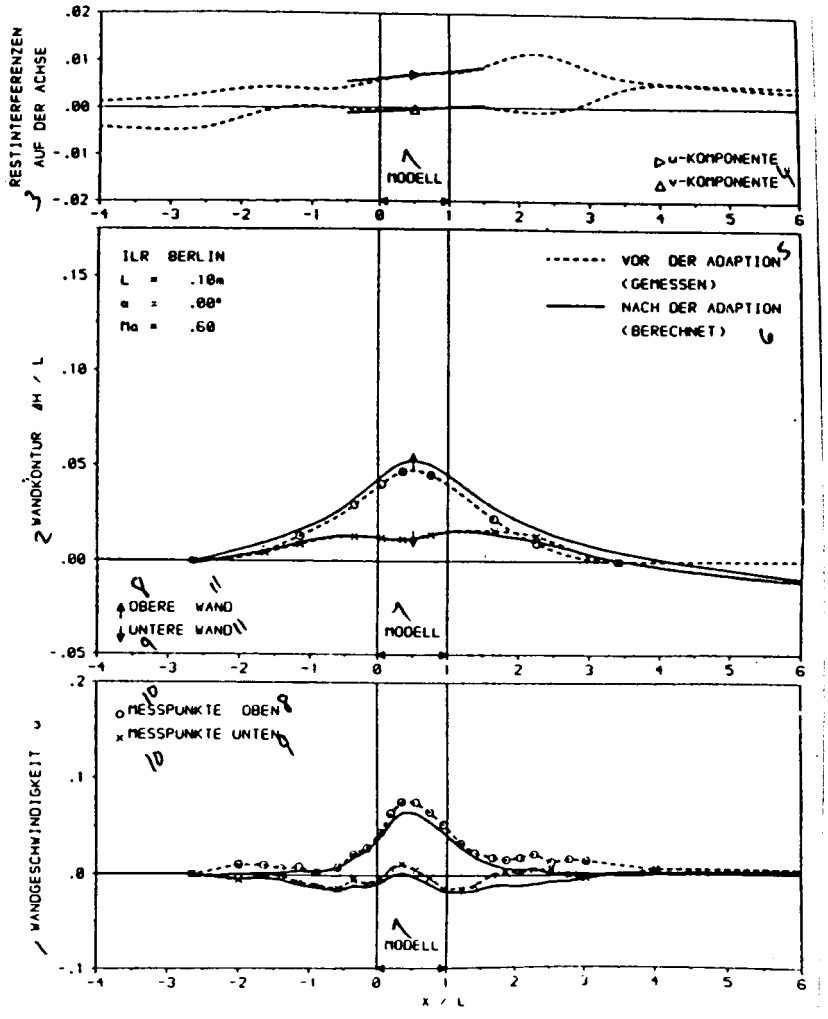

Fig. 21: Measurement Point Ma = 0.60 and alpha = 0.00 by TU Berlin

Key: 1-wall velocity 2-wall contour 3-residual interferences on the axis 4-component 5-before adaptation (measured) 6-after adaptation (calculated) 7-model 8-upper 9-lower 10-measured point 11-wall

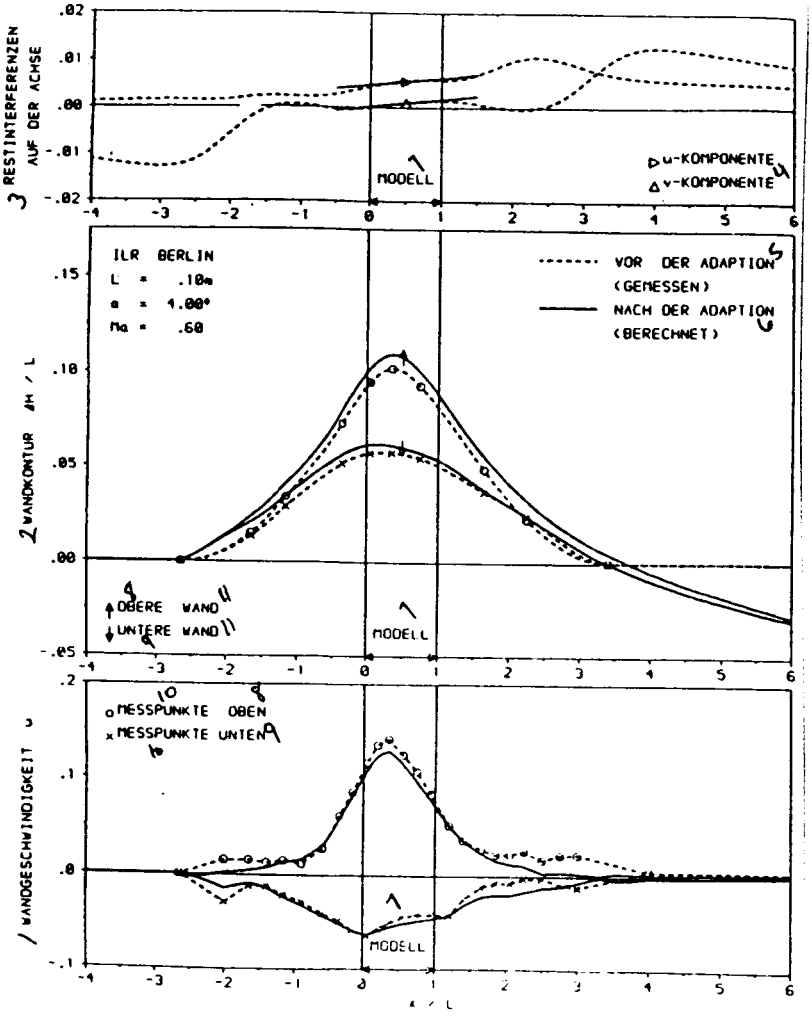

Fig. 22: Measurement Point Ma = 0.60 and alpha = 4.00 by TU Berlin

Key: 1-wall velocity 2-wall contour 3-residual interferences on the axis 4-component 5-before adaptation (measured) 6-after adaptation (calculated) 7-model 8-upper 9-lower 10-measured point 11-wall

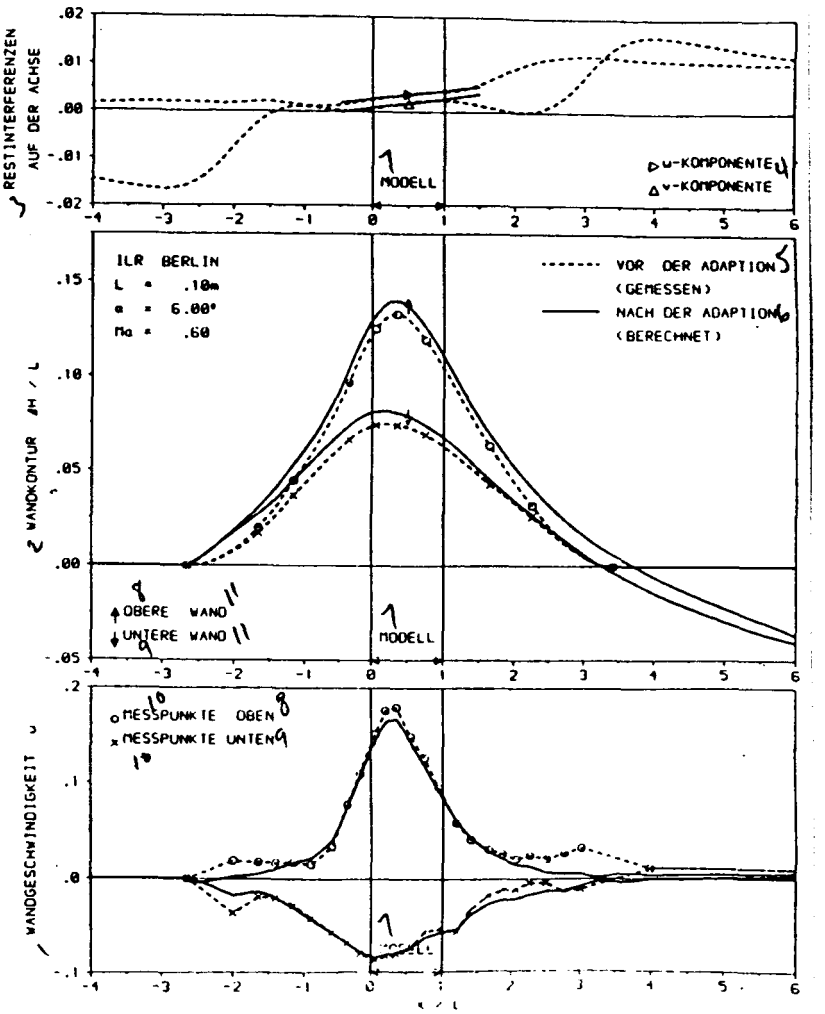

Fig. 23: Measurement Point Ma = 0.60 and alpha = 6.00 by TU Berlin

Key: 1-wall velocity 2-wall contour 3-residual interferences on the axis 4-component 5-before adaptation (measured) 6-after adaptation (calculated) 7-model 8-upper 9-lower 10-measured point 11-wall

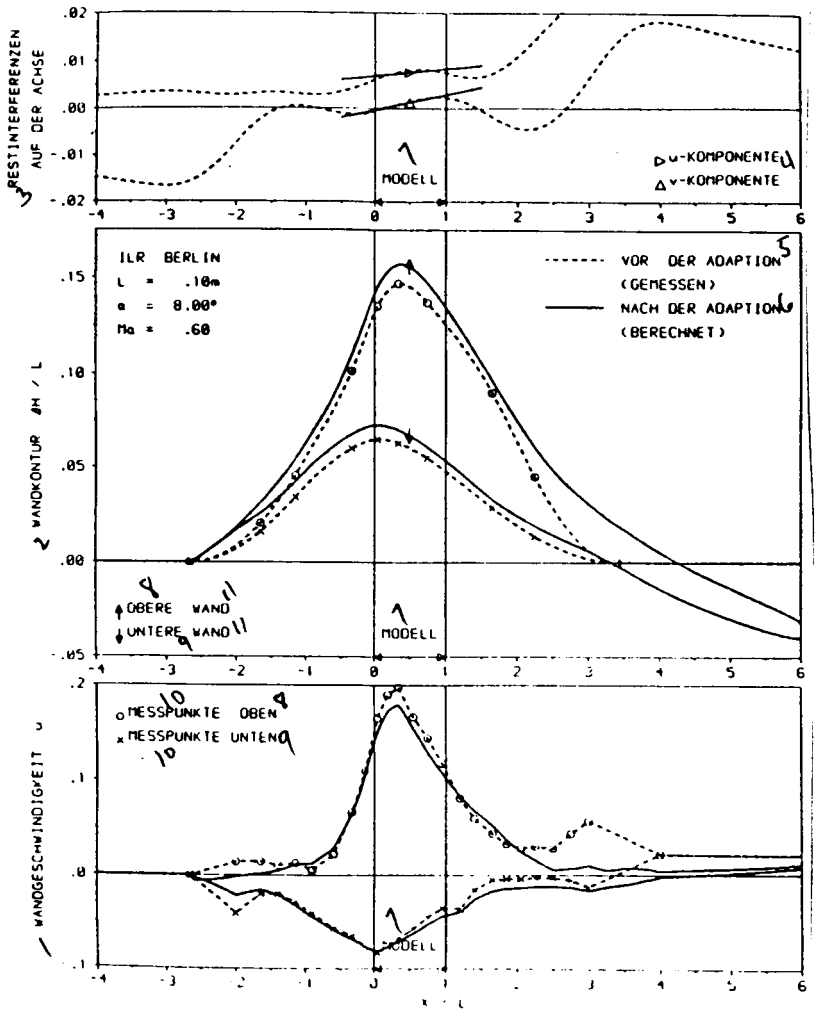

Fig. 24: Measurement Point Ma = 0.60 and alpha = 8.00 by TU Berlin

Key: 1-wall velocity 2-wall contour 3-residual interferences on the axis 4-component 5-before adaptation (measured) 6-after adaptation (calculated) 7-model 8-upper 9-lower 10-measured point 11-wall

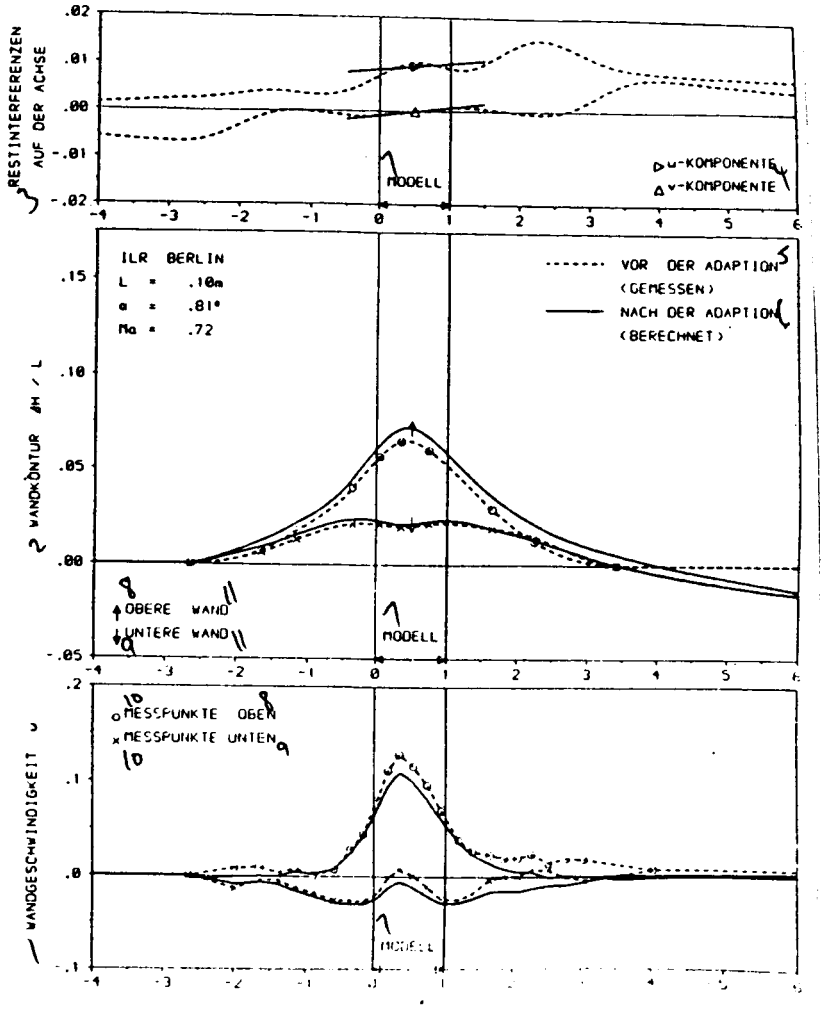

Fig. 25: Measurement Point Ma = 0.72 and alpha = 0.81 by TU Berlin

Key: 1-wall velocity 2-wall contour 3-residual interferences on the axis 4-component 5-before adaptation (measured) 6-after adaptation (calculated) 7-model 8-upper 9-lower 10-measured point 11-wall

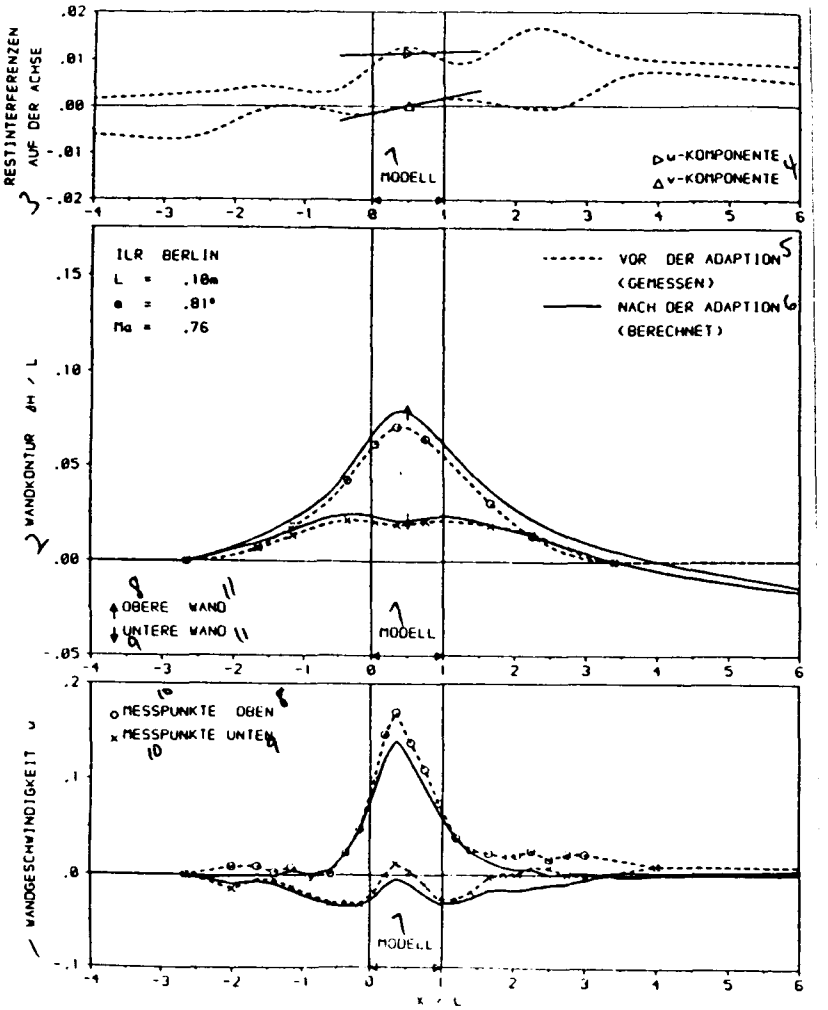

Fig. 26: Measurement Point Ma = 0.76 and alpha = 0.81 by TU Berlin

Key: 1-wall velocity 2-wall contour 3-residual interferences on the axis 4-component 5-before adaptation (measured) 6-after adaptation (calculated) 7-model 8-upper 9-lower 10-measured point 11-wall

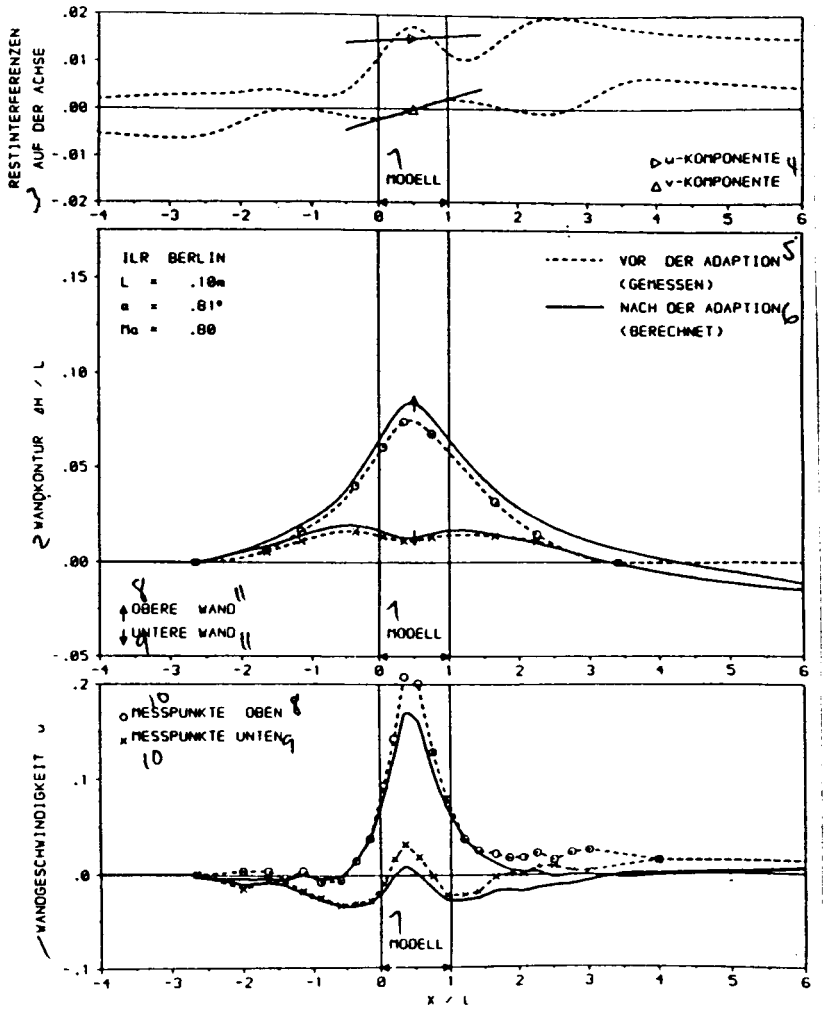

Fig. 27: Measurement Point Ma = 0.80 and alpha = 0.81 by TU Berlin

Key: 1-wall velocity 2-wall contour 3-residual interferences on the axis 4-component 5-before adaptation (measured) 6-after adaptation (calculated) 7-model 8-upper 9-lower 10-measured point 11-wall

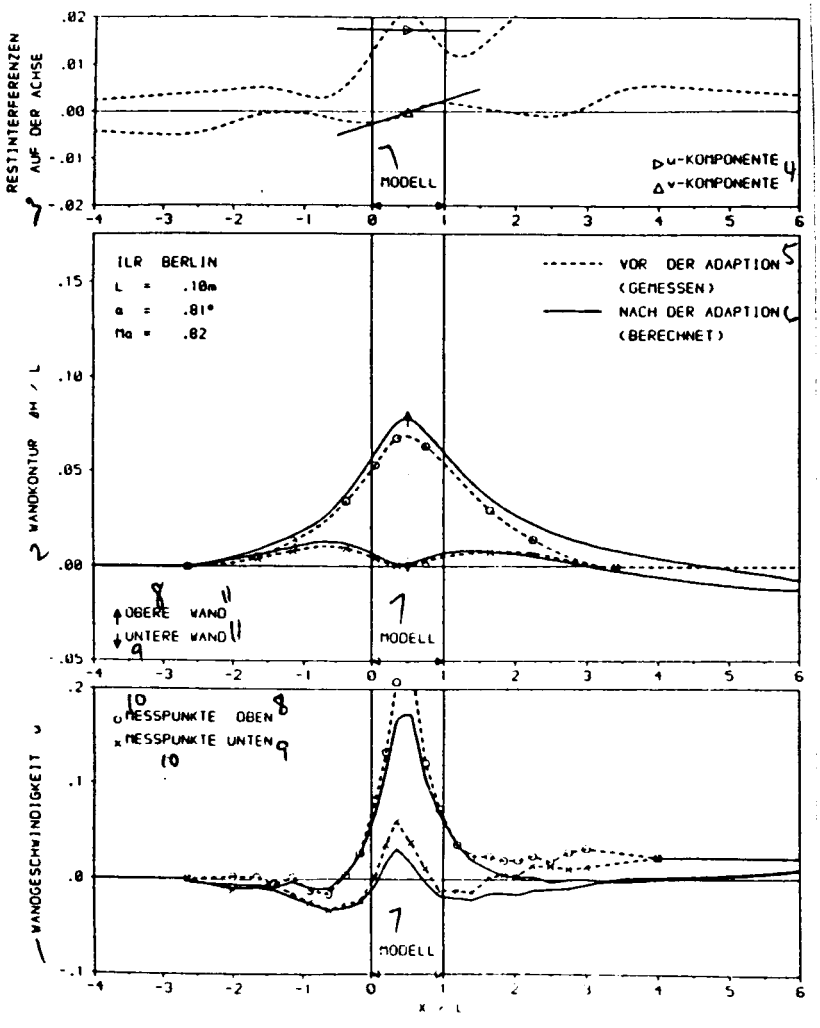

Fig. 28: Measurement Point Ma = 0.82 and alpha = 0.81 by TU Berlin

Key: 1-wall velocity 2-wall contour 3-residual interferences on the axis 4-component 5-before adaptation (measured) 6-after adaptation (calculated) 7-model 8-upper 9-lower 10-measured point 11-wall

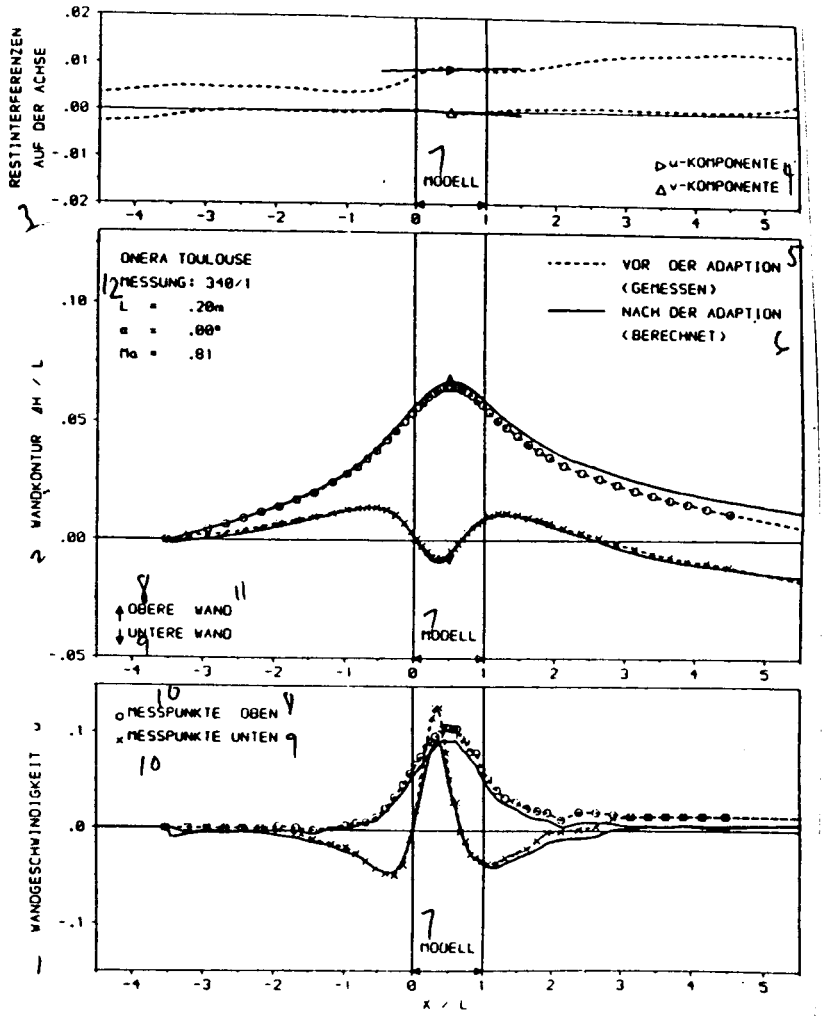

Fig. 29: Measurement Point Ma = 0.81 and alpha = 0.0 (1st Iteration) by T2 Toulouse

Key: 1-wall velocity 2-wall contour 3-residual interferences on the axis 4-component 5-before adaptation (measured) 6-after adaptation (calculated) 7-model 8-upper 9-lower 10-measured point 11-wall 12-measurement

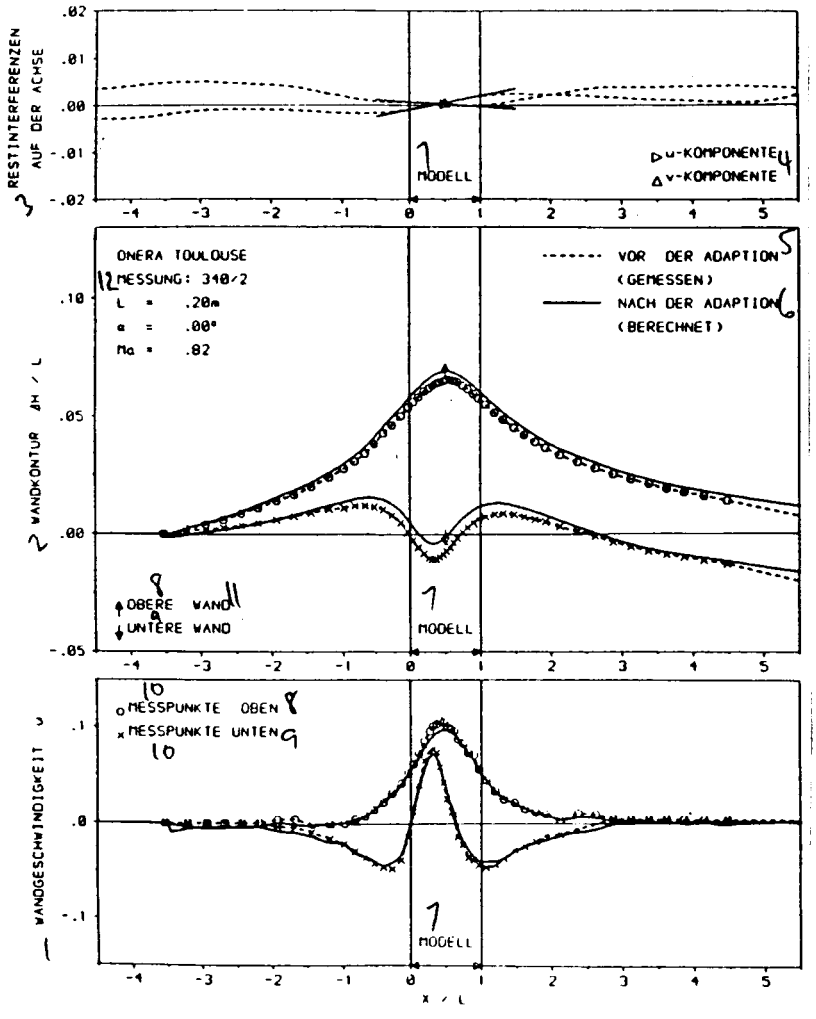

Fig. 30: Measurement Point Ma = 0.81 and alpha = 0.0 (2nd Iteration) by T2 Toulouse

Key: 1-wall velocity 2-wall contour 3-residual interferences on the axis 4-component 5-before adaptation (measured) 6-after adaptation (calculated) 7-model 8-upper 9-lower 10-measured point 11-wall 12-measurement

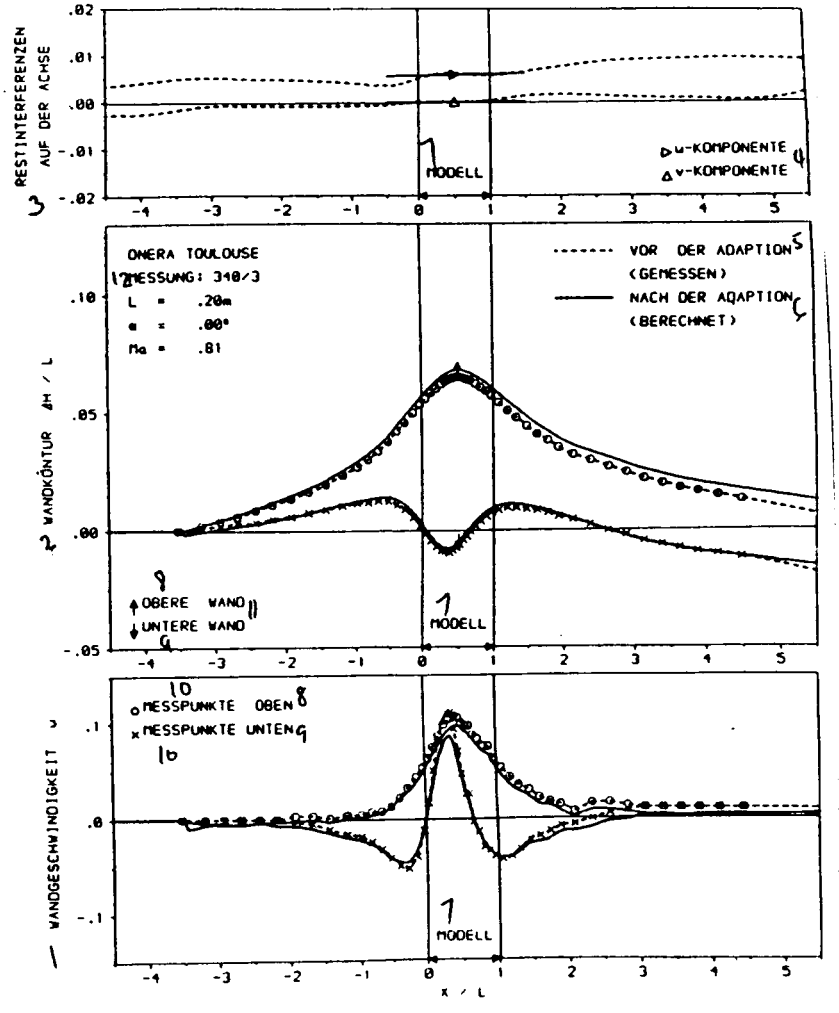

Fig. 31: Measurement Point Ma = 0.81 and alpha = 0.0 (3rd Iteration) by T2 Toulouse

Key: 1-wall velocity 2-wall contour 3-residual interferences on the axis 4-component 5-before adaptation (measured) 6-after adaptation (calculated) 7-model 8-upper 9-lower 10-measured point 11-wall 12-measurement

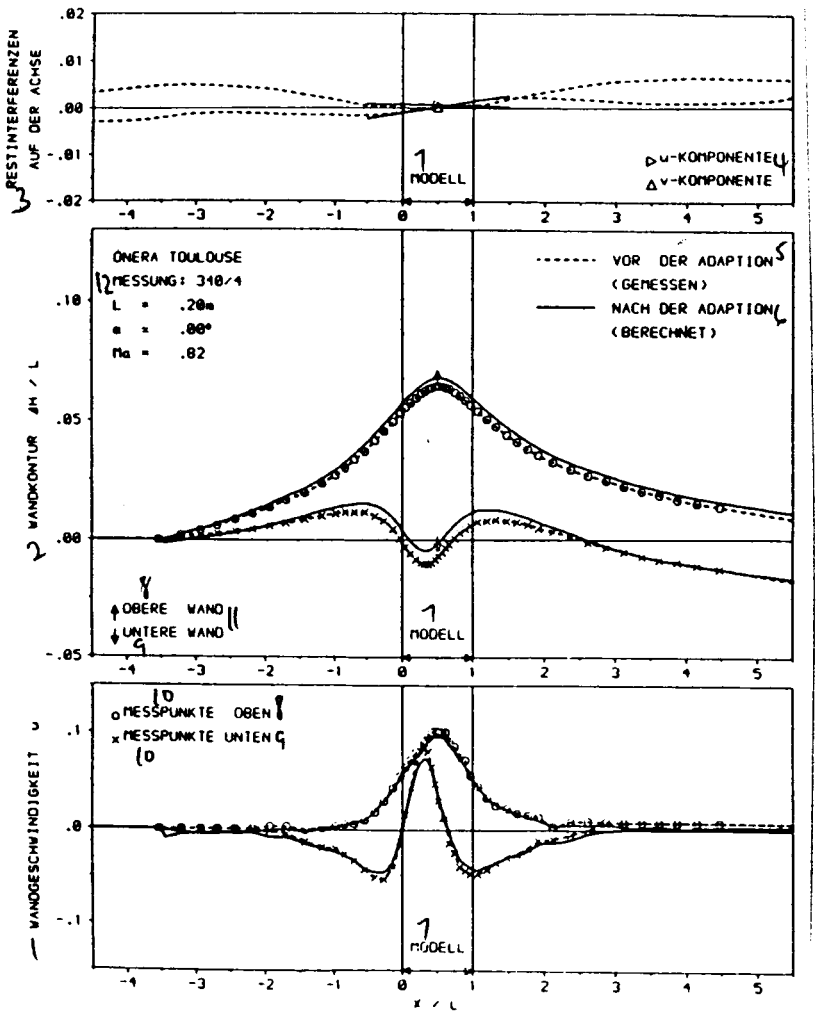

Fig. 32: Measurement Point Ma = 0.81 and alpha = 0.0 (4th Iteration) by T2 Toulouse

Key: 1-wall velocity 2-wall contour 3-residual interferences on the axis 4-component 5-before adaptation (measured) 6-after adaptation (calculated) 7-model 8-upper 9-lower 10-measured point 11-wall 12-measurement

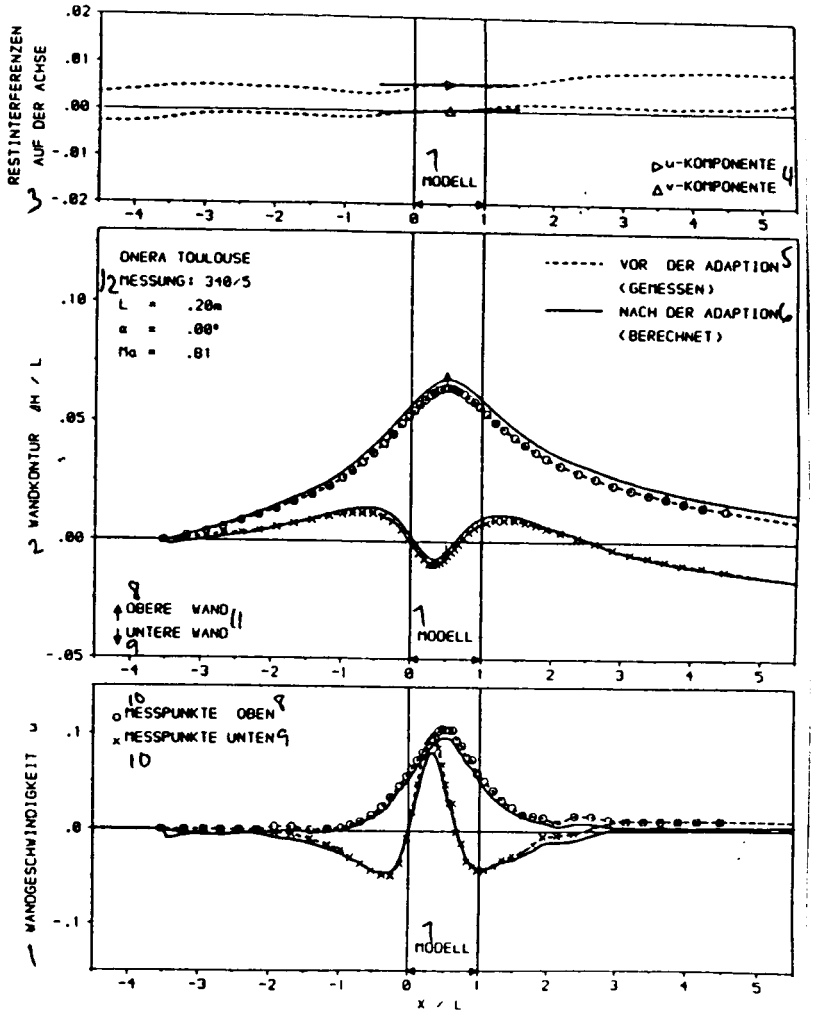

Fig. 33: Measurement Point Ma = 0.81 and alpha = 0.0 (5th Iteration) by T2 Toulouse

Key: 1-wall velocity 2-wall contour 3-residual interferences on the axis 4-component 5-before adaptation (measured) 6-after adaptation (calculated) 7-model 8-upper 9-lower 10-measured point 11-wall 12-measurement

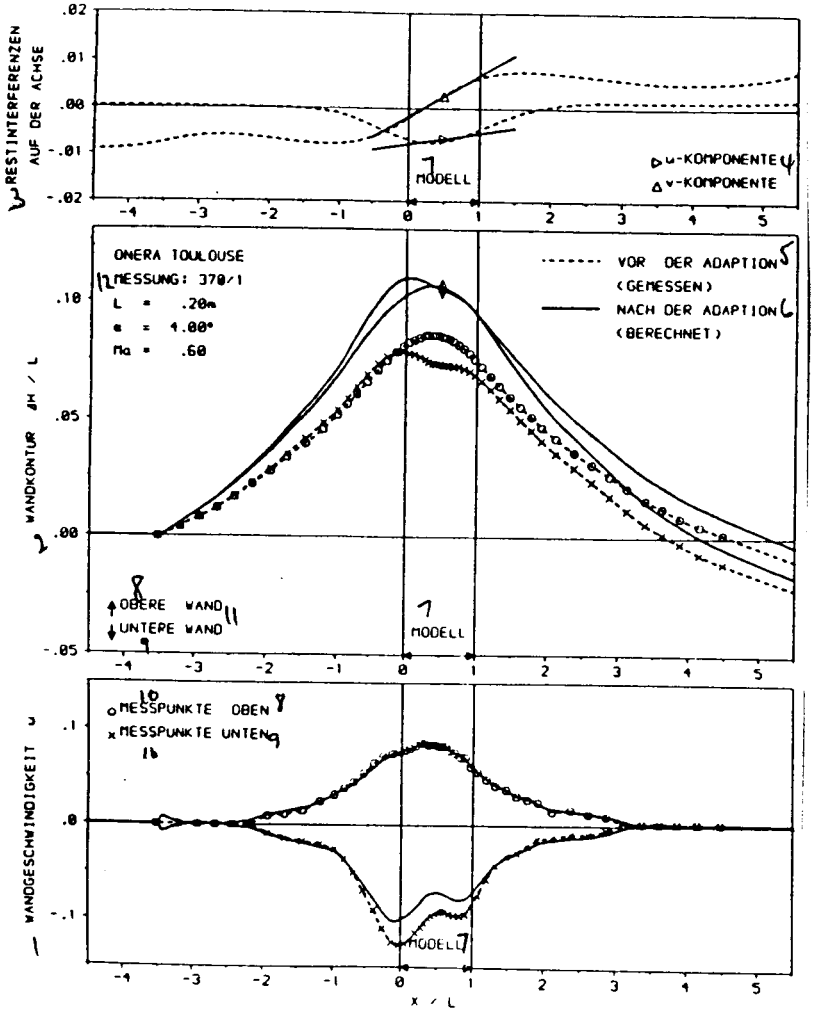

Fig. 34: Measurement Point Ma = 0.60 and alpha = 4.0 (1st Iteration) by T2 Toulouse

Key: 1-wall velocity 2-wall contour 3-residual interferences on the axis 4-component 5-before adaptation (measured) 6-after adaptation (calculated) 7-model 8-upper 9-lower 10-measured point 11-wall 12-measurement

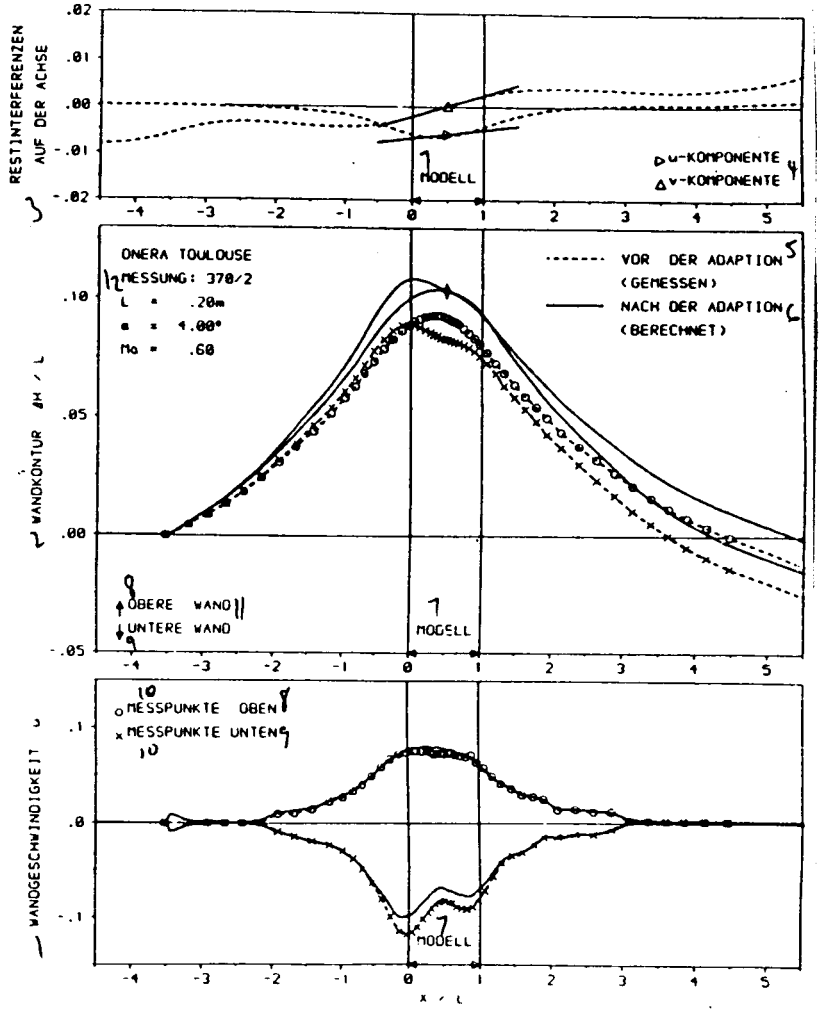

Fig. 35: Measurement Point Ma = 0.60 and alpha = 4.0 (2nd Iteration) by T2 Toulouse

Key: 1-wall velocity 2-wall contour 3-residual interferences on the axis 4-component 5-before adaptation (measured) 6-after adaptation (calculated) 7-model 8-upper 9-lower 10-measured point 11-wall 12-measurement

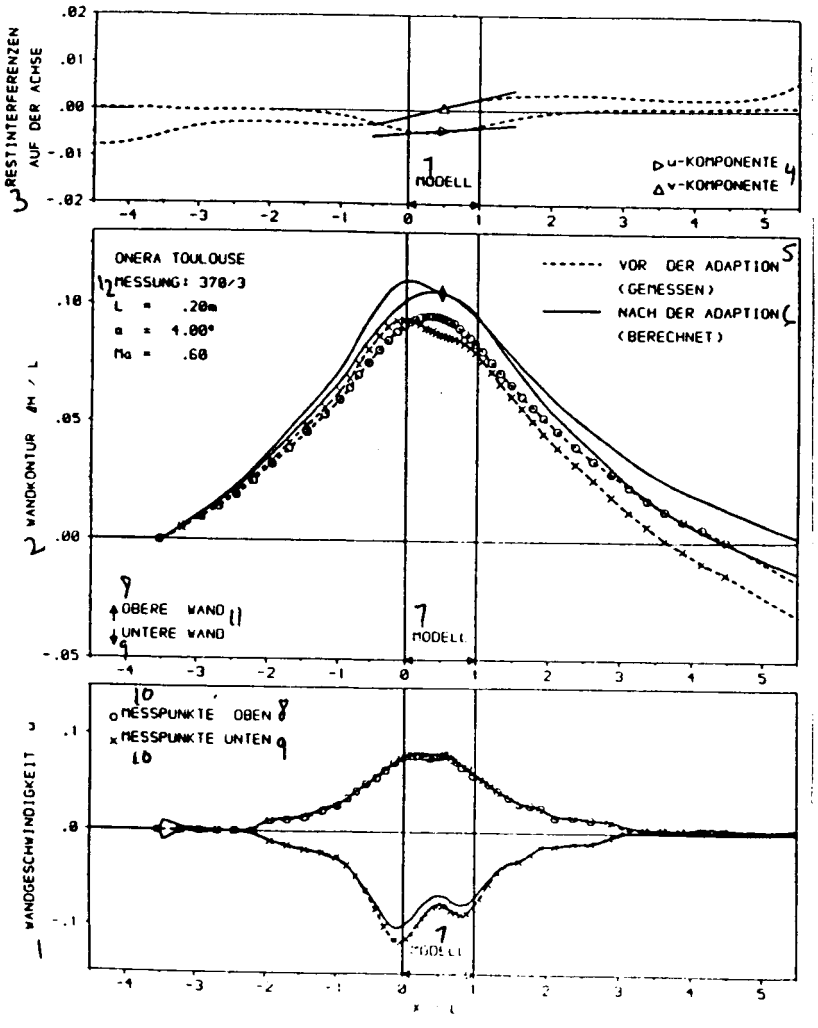

Fig. 36: Measurement Point Ma = 0.60 and alpha = 4.0 (3rd Iteration) by T2 Toulouse

Key: 1-wall velocity 2-wall contour 3-residual interferences on the axis 4-component 5-before adaptation (measured) 6-after adaptation (calculated) 7-model 8-upper 9-lower 10-measured point 11-wall 12-measurement

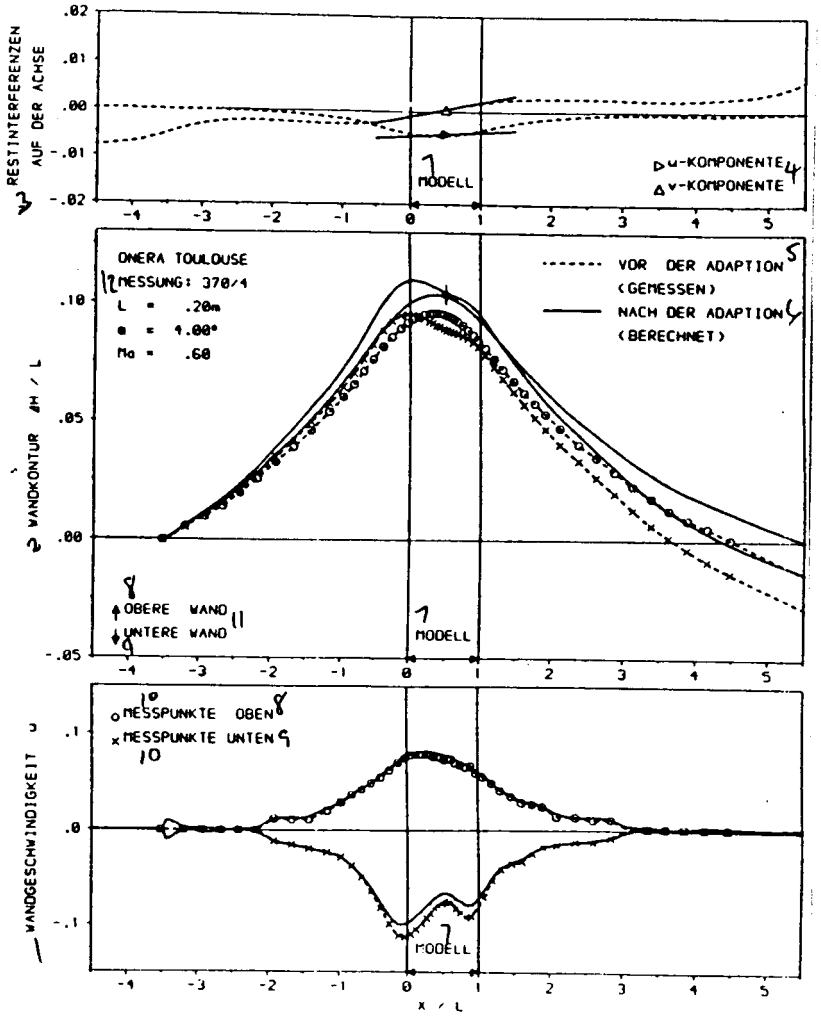

Fig. 37: Measurement Point Ma = 0.60 and alpha = 4.0 (4th Iteration) by T2 Toulouse

Key: 1-wall velocity 2-wall contour 3-residual interferences on the axis 4-component 5-before adaptation (measured) 6-after adaptation (calculated) 7-model 8-upper 9-lower 10-measured point 11-wall 12-measurement

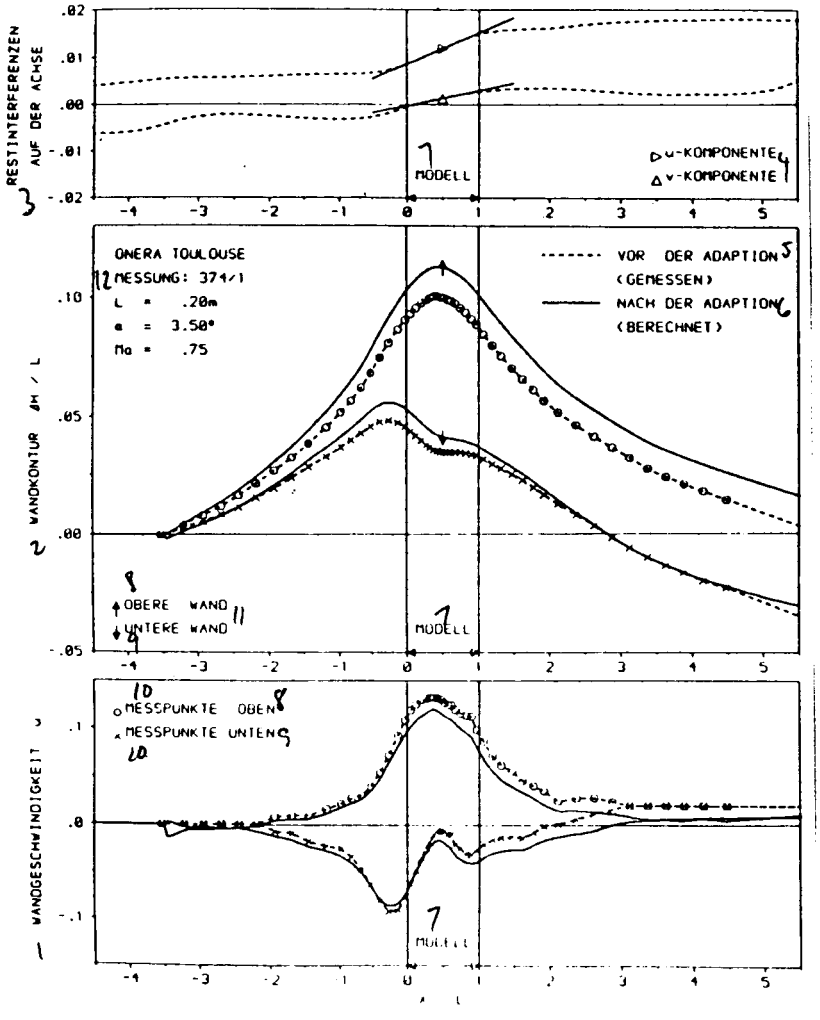

Fig. 38: Measurement Point Ma = 0.75 and alpha = 3.5 (1st Iteration) by T2 Toulouse

Key: 1-wall velocity 2-wall contour 3-residual interferences on the axis 4-component 5-before adaptation (measured) 6-after adaptation (calculated) 7-model 8-upper 9-lower 10-measured point 11-wall 12-measurement

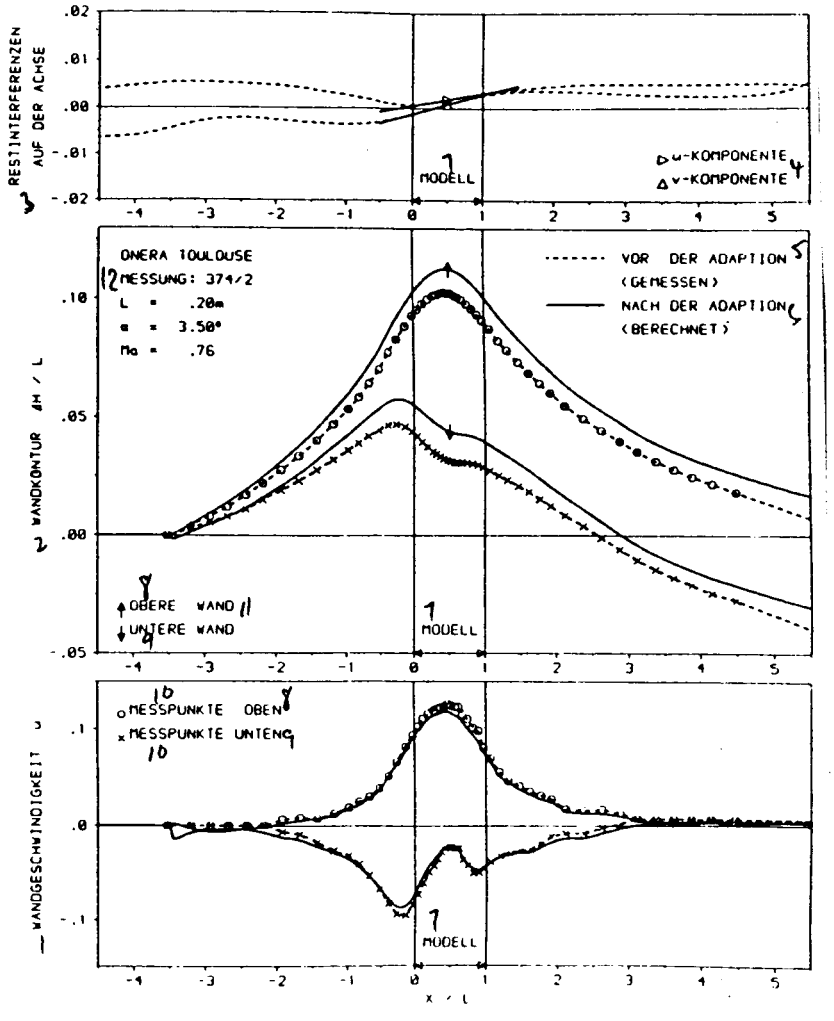

Fig. 39: Measurement Point Ma = 0.75 and alpha = 3.5 (2nd Iteration) by T2 Toulouse

Key: 1-wall velocity 2-wall contour 3-residual interferences on the axis 4-component 5-before adaptation (measured) 6-after adaptation (calculated) 7-model 8-upper 9-lower 10-measured point 11-wall 12-measurement

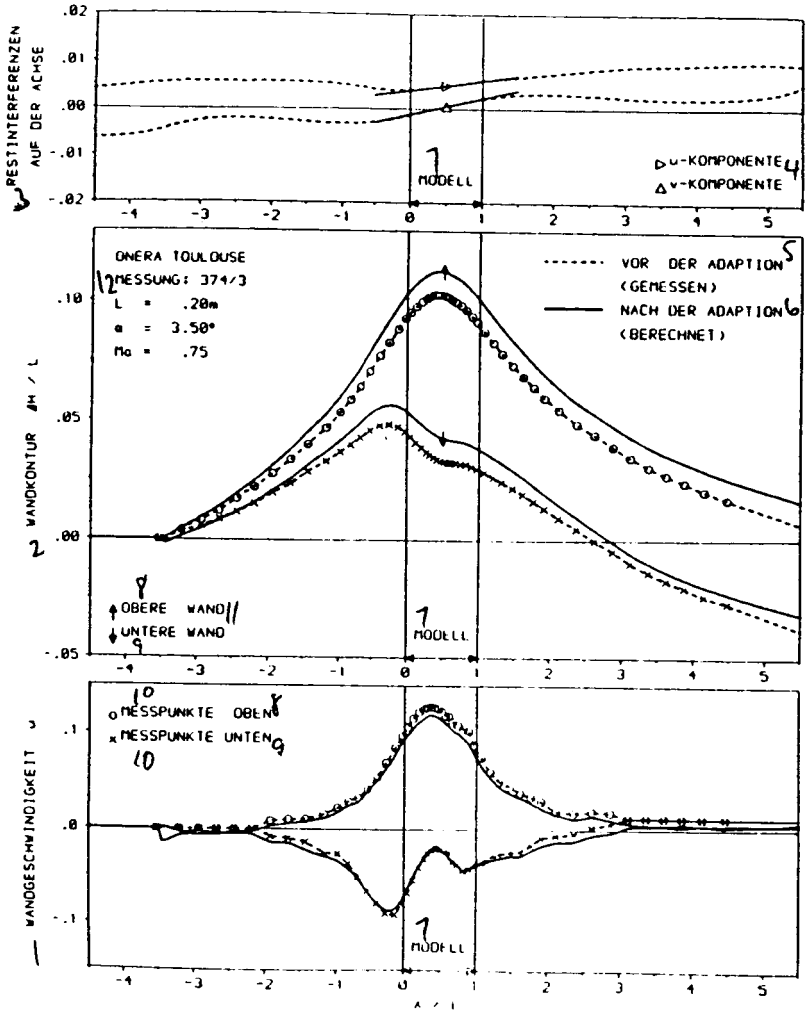

Fig. 40: Measurement Point Ma = 0.75 and alpha = 3.5 (3rd Iteration) by T2 Toulouse

Key: 1-wall velocity 2-wall contour 3-residual interferences on the axis 4-component 5-before adaptation (measured) 6-after adaptation (calculated) 7-model 8-upper 9-lower 10-measured point 11-wall 12-measurement

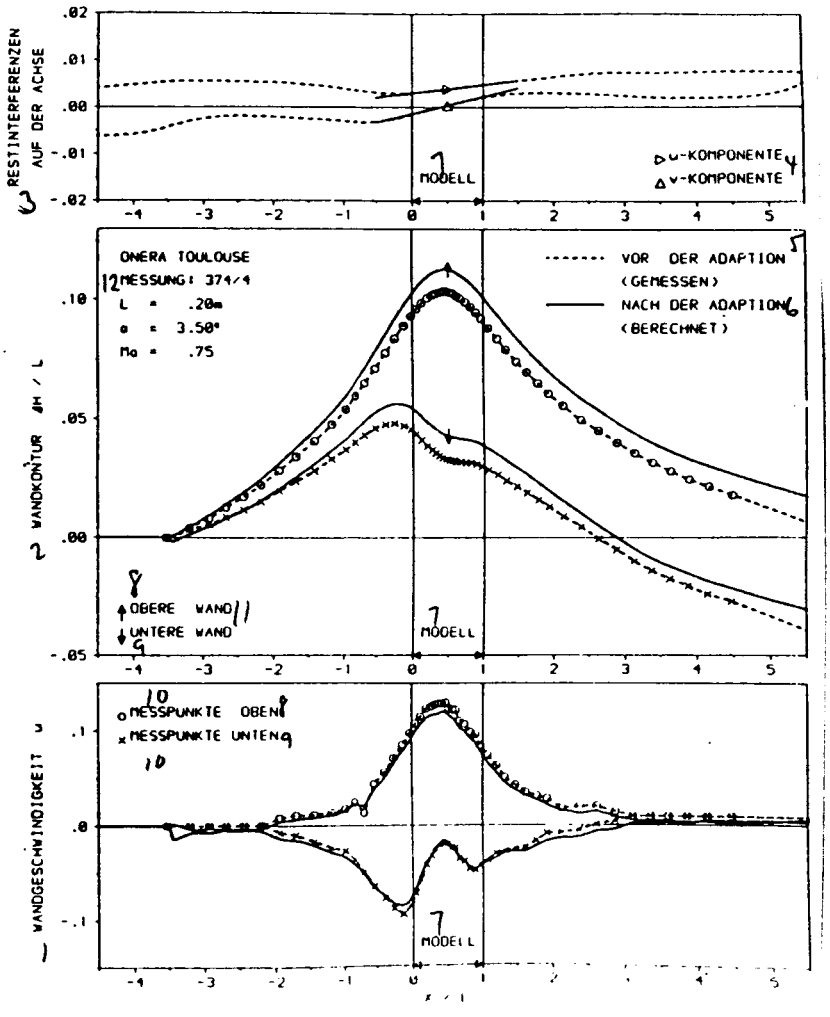

Fig. 41: Measurement Point Ma = 0.75 and alpha = 3.5 (4th Iteration) by T2 Toulouse

Key: 1-wall velocity 2-wall contour 3-residual interferences on the axis 4-component 5-before adaptation (measured) 6-after adaptation (calculated) 7-model 8-upper 9-lower 10-measured point 11-wall 12-measurement

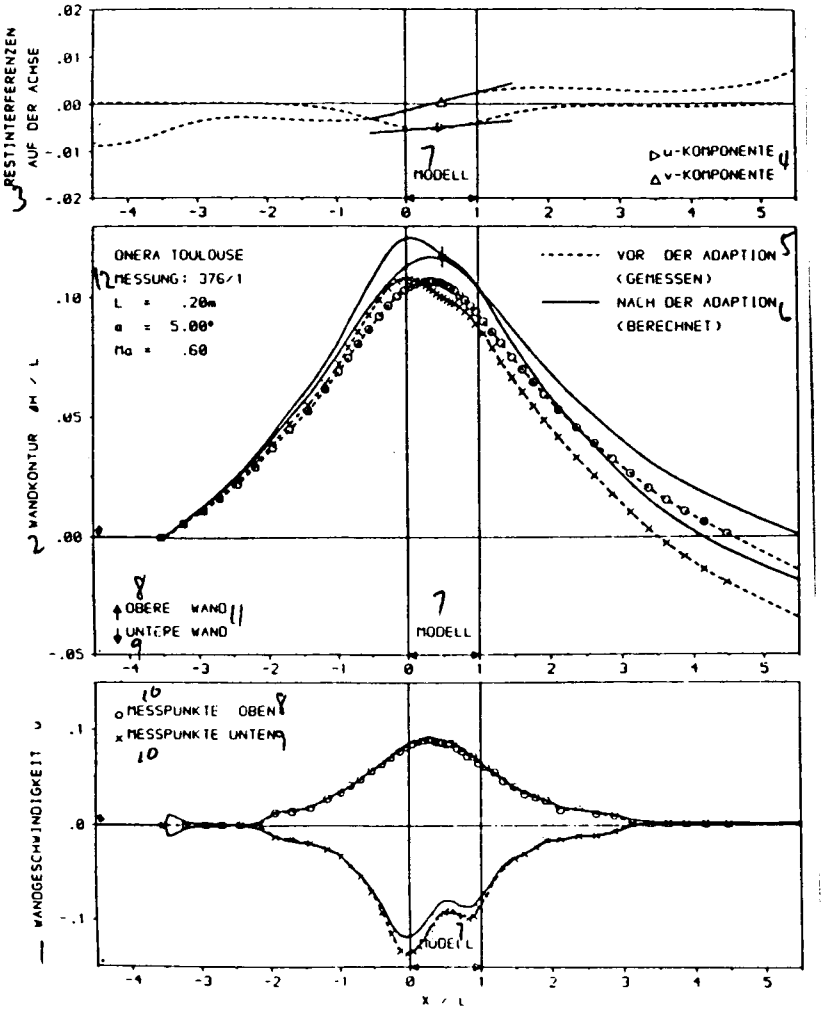

Fig. 42: Measurement Point Ma = 0.60 and alpha = 5.0 (1st Iteration) by T2 Toulouse

Key: 1-wall velocity 2-wall contour 3-residual interferences on the axis 4-component 5-before adaptation (measured) 6-after adaptation (calculated) 7-model 8-upper 9-lower 10-measured point 11-wall 12-measurement

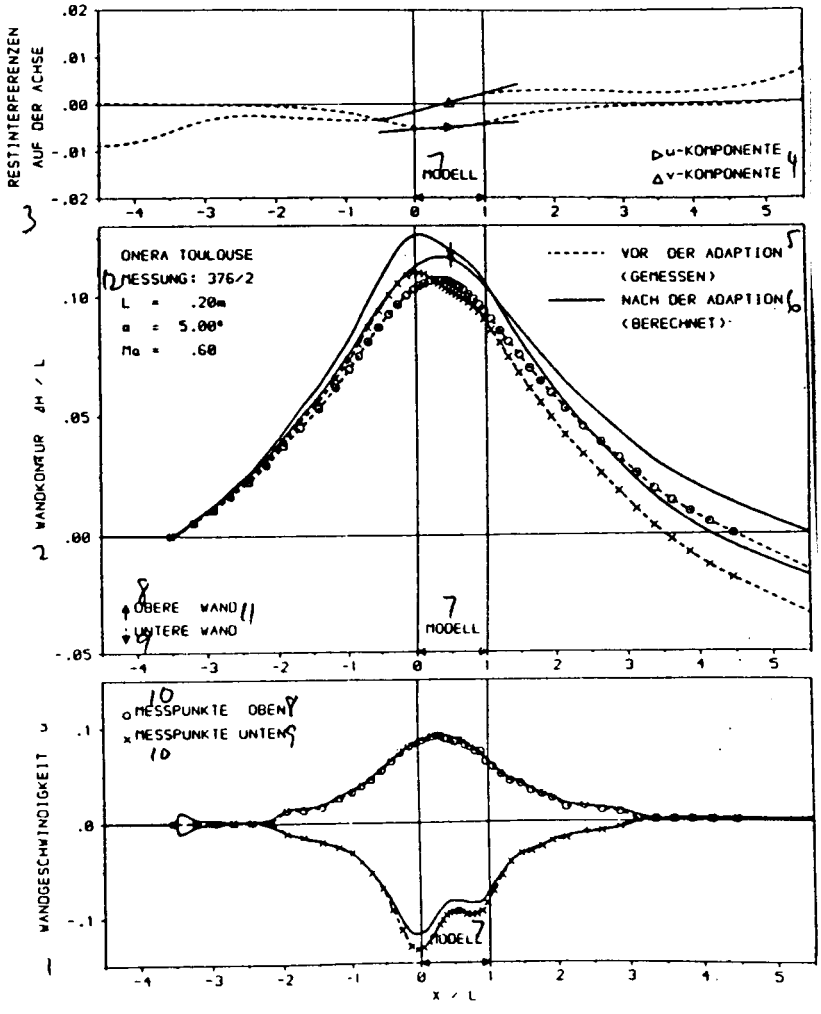

Fig. 43: Measurement Point Ma = 0.60 and alpha = 5.0 (2nd Iteration) by T2 Toulouse

Key: 1-wall velocity 2-wall contour 3-residual interferences on the axis 4-component 5-before adaptation (measured) 6-after adaptation (calculated) 7-model 8-upper 9-lower 10-measured point 11-wall 12-measurement

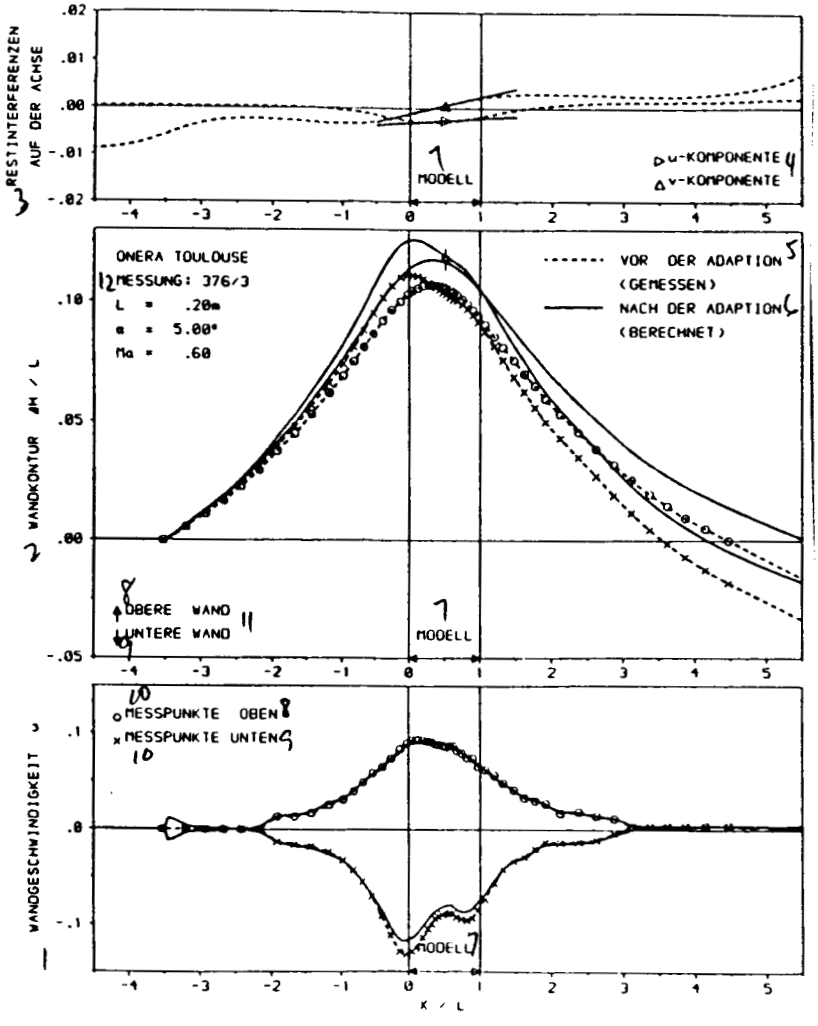

Fig. 44: Measurement Point Ma = 0.60 and alpha = 5.0 (3rd Iteration) by T2 Toulouse

Key: 1-wall velocity 2-wall contour 3-residual interferences on the axis 4-component 5-before adaptation (measured) 6-after adaptation (calculated) 7-model 8-upper 9-lower 10-measured point 11-wall 12-measurement

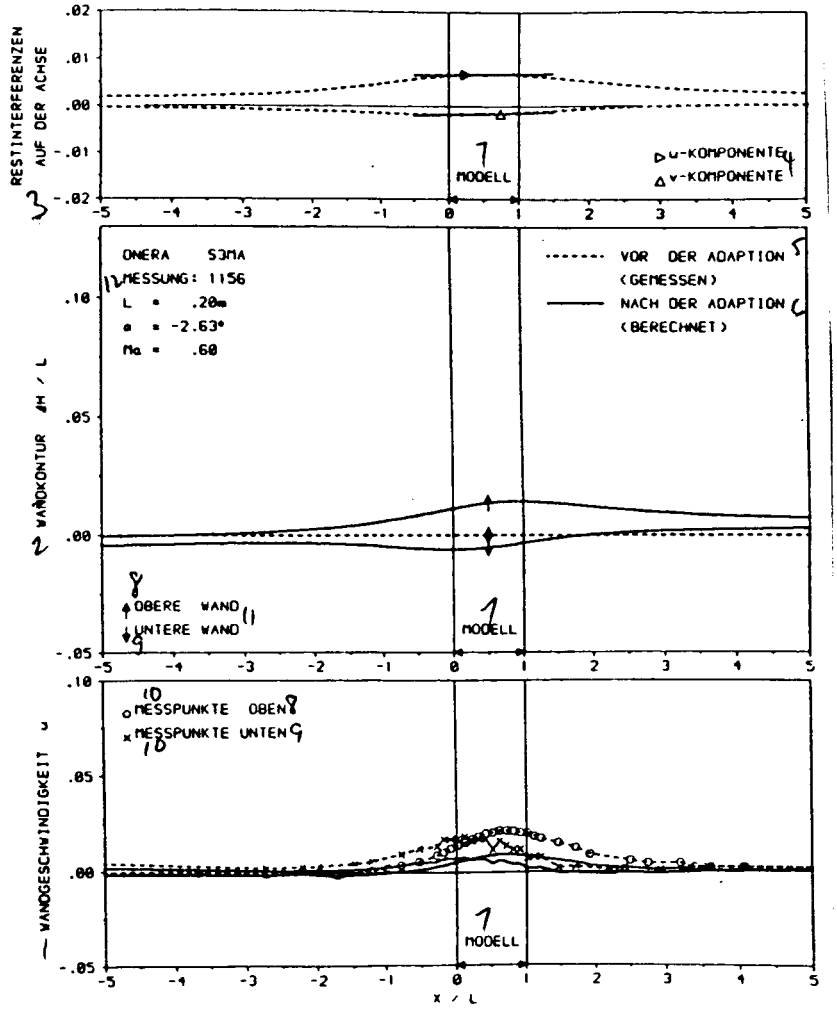

Fig. 45: Measurement Point Ma = 0.60 and alpha = -2.63 by S3 Modane

Key: 1-wall velocity 2-wall contour 3-residual interferences on the axis 4-component 5-before adaptation (measured) 6-after adaptation (calculated) 7-model 8-upper 9-lower 10-measured point 11-wall 12-measurement

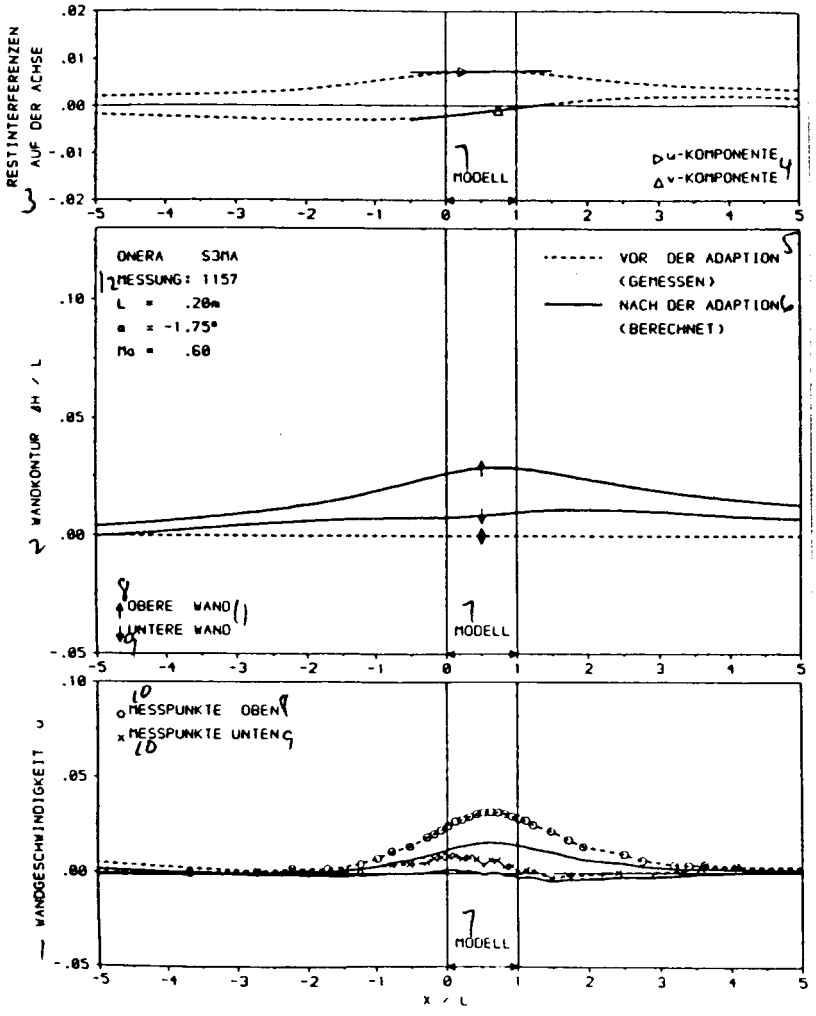

Fig. 46: Measurement Point Ma = 0.60 and alpha = -1.75 by S3 Modane

Key: 1-wall velocity 2-wall contour 3-residual interferences on the axis 4-component 5-before adaptation (measured) 6-after adaptation (calculated) 7-model 8-upper 9-lower 10-measured point 11-wall 12-measurement

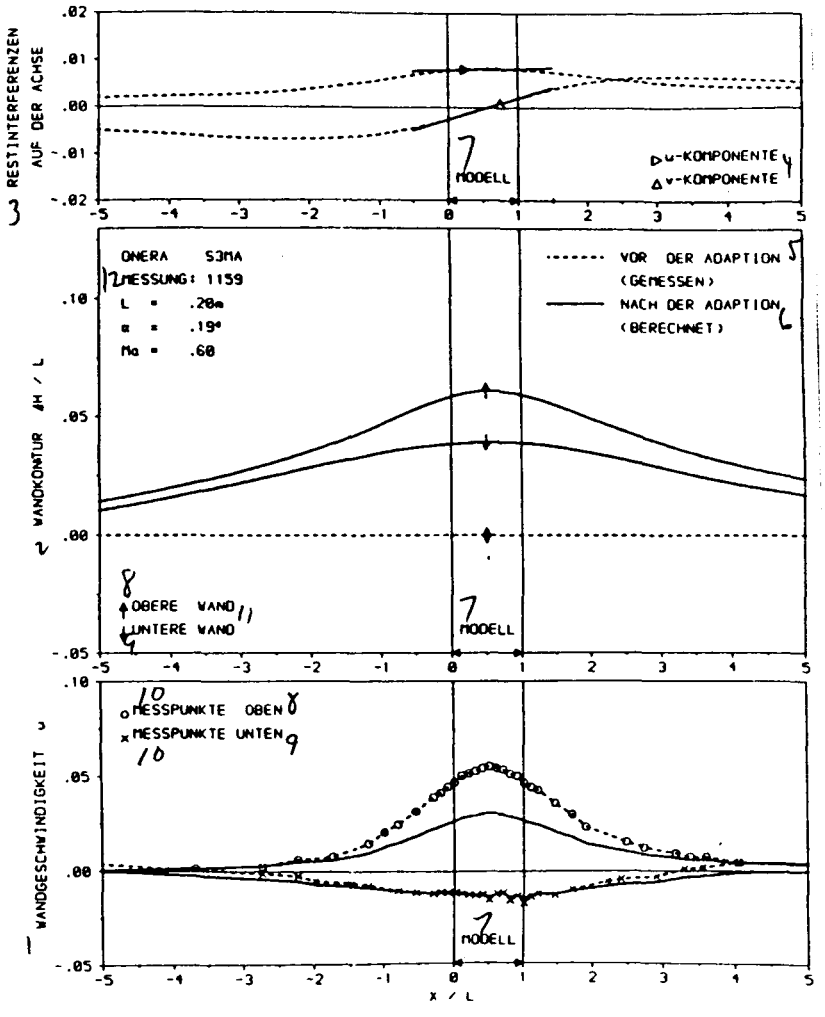

Fig. 47: Measurement Point Ma = 0.60 and alpha = 0.19 by S3 Modane

Key: 1-wall velocity 2-wall contour 3-residual interferences on the axis 4-component 5-before adaptation (measured) 6-after adaptation (calculated) 7-model 8-upper 9-lower 10-measured point 11-wall 12-measurement

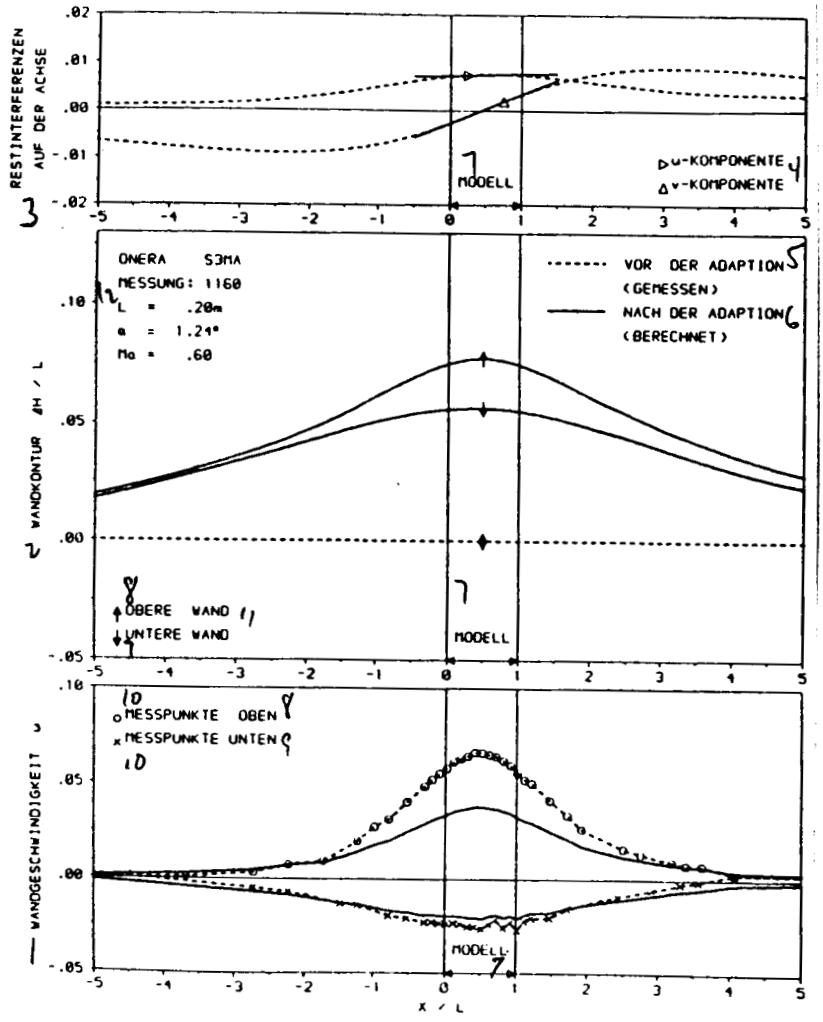

Fig. 48: Measurement Point Ma = 0.60 and alpha = 1.24 by S3 Modane

Key: 1-wall velocity 2-wall contour 3-residual interferences on the axis 4-component 5-before adaptation (measured) 6-after adaptation (calculated) 7-model 8-upper 9-lower 10-measured point 11-wall 12-measurement

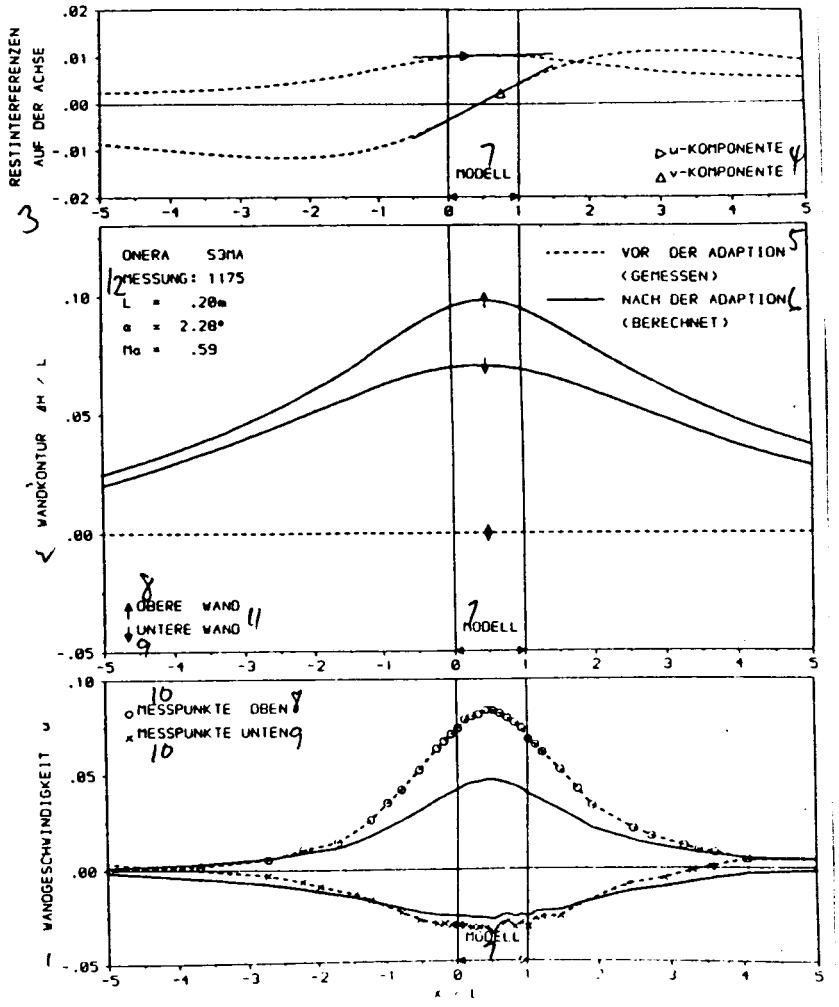

Fig. 49: Measurement Point Ma = 0.60 and alpha = 2.28 by S3 Modane

Key: 1-wall velocity 2-wall contour 3-residual interferences on the axis 4-component 5-before adaptation (measured) 6-after adaptation (calculated) 7-model 8-upper 9-lower 10-measured point 11-wall 12-measurement